Lunds Universitets Naturgeografiska Institution

Seminarieuppsatser Nr. 74

Estimation of Leaf Area Index in Southern Sweden with Optical Modelling and a Landsat 7 ETM+Scene

Pontus Olofsson & Richard Stenström

2000

Department of Physical Geography,
Lund University
Sölvegatan 13, S-221 00 Lund,
Sweden

Abstract

Canopy reflectance models are used as a means of estimating vegetation parameters and simulating reflectance signatures of vegetation surfaces. A forest canopy reflectance model is tested on deciduous forest collections in southern Sweden. A sensitivity analysis is performed to study how large influence each parameter has on the simulated reflectance. Thorough field measurements of the forest collections are done were the structural parameters are measured. The branch area index and leaf area index are measured with the Li-Cor LAI-2000 optical sensor, and two methods are tested to obtain leaf area index from effective leaf area index. The field data are used together with LOPEX leaf biophysical data to simulate the reflectance from the forest collections. The obtained reflectance is correlated against atmospheric influence corrected Landsat 7 ETM reflectance data. Atmospheric correction of the satellite data is done with a radiative transfer model named 6S, and atmospheric input data from SMHI (the Swedish Meteorological and Hydrological Institute). The forest model is further tested in inverse mode to obtain LAI. The inverted LAI values are compared to the measured ones. A sensitivity analysis showed that crown radius, chlorophyll content and leaf structural parameter are the most important parameters. LAI, BAI and stand density showed moderate importance while the other parameters showed low influence on the calculated reflectance.

The correlation between modelled and measured reflectance was very low with the best correlation in ETM 5 (r = 0.55). The inversion of the model yielded low correlations except for collections with one size class. These collections proved to be more easily modelled.

Acknowledgements

This thesis is the final examination in the mathematical-natural science education program at the Department of Physical Geography, Lund University. PhD Lars Eklundh was our instructor.

We wish to thank the following persons for supplying material and ideas.

Lars Eklundh	Department of Physical Geography, Lund University.
Jonas Ardö	Department of Physical Geography, Lund University.
Tomas Landelius	Forskning och utveckling, SMHI.
Thomas Person	Forskning och utveckling, SMHI.
Brian Hosgood	Joint Research Centre, Italy.

Lund University contact addresses

Pontus Olofsson
Ällingavägen 22:21
227 34 Lund
nge95pol@student.lu.se

Richard Stenström
Drottninggatan 67
252 22 Helsingborg
richards80@hotmail.com

Lars Eklundh
Dep. of Physical Geography
Lund University
Box 118, 221 00 Lund
Lars.Eklundh@natgeo.lu.se

Jonas Ardö
Dep. of Physical Geography
Lund University
Box 118, 221 00 Lund
Jonas.Ardo@natgeo.lu.se

Dictionary

Aerosol – Tiny suspended particles or liquid droplets that enters the atmosphere from either anthropogenic or natural sources (Ahrens, 1994).

Albedo – ”the percent of radiation returning from a surface compared to that which strikes it” (Ahrens, 1994).

BAI - Branch Area Index, defined as one half the total surface area of branches per unit ground surface area (Kucharik *et al.*, 1998).

BAI_e - Effective BAI, the product of BAI and a non-randomness factor for branches (Kucharik *et al.*, 1998).

Covariance – as an extension of the variance, the covariance of two variables x and y is the expectation of (x- μ_x)(y-μ_y), where μ_x and μ_y are means of x and y (Considine, 1989). Used for expressing interdependence between variables (CGCC glossary).

Diffuse radiation – occurs when rough surface scatters the energy in (more or less) all directions (Campbell, 1996).

Exoatmospheric irradiance – irradiance in the outermost portion of the atmosphere (Ahrens, 1994).

Irradiance – measures radiation that strikes a surface, [radiant flux per unit area] (Campbell, 1996).

LAI - Leaf Area Index, it is defined as one-half the surface area of leaves per unit ground surface [m^2/m^2] (Kucharik *et al.*, 1998).

LAI_e - Effective LAI, indirect measure of all foliage in a canopy based on canopy gap fraction technique including a non-randomness factor for the canopy foliage elements(Kucharik *et al.*, 1998).

Lambertian surface/case – A perfect diffuse reflector that would have equal brightness when observed from any direction (Campbell, 1996).

Landsat MSS, TM and ETM – US land observations satellites. Landsat 1, MSS-sensor (geometrical res. of 79 × 79 m), launched in 1972. Landsat 4, TM-sensor (geometrical res. of 30 × 30 m), launched 1982 (Campbell, 1996). Landsat 7, ETM-sensor (geometrical res. of 30 × 30 m, but with a higher radiometric res. then the TM- sensor), launched in 1998.

Matrix – a p×n matrix is a rectangular scheme of numbers with *j* numbers of rows and *k* numbers of columns; a_{jk} is called a matrix element (Andersson, 1985).

Optical thickness – the vertical attenuation coefficient $\tau(\lambda)=\beta\cdot\lambda^{-x}$, where β is the Ångström turbidity factor and λ is the wavelength. β can be estimated from the ratio of diffuse to total irradiance (Kuusk, 1994).

PAI - Total plant area index (Kucharik *et al.*, 1998).

Photon – "a discrete quantity of energy that can be thought of as a packet of electromagnetic radiation traveling with the speed of light" (Ahrens, 1994)

Rayleigh scattering – occurs in the atmosphere when a particles diameter is small relative the wavelength radiation (Campbell, 1996).

Solar azimuth angle, α – defined as $\cos(\alpha)=(\sin(\delta_s)-\sin(\phi)\cdot\sin(\varsigma))/(\cos(\phi)\cdot\sin(\varsigma))$, where δ_s is the sun declination angle (the tilt of the earth's axis), ϕ is the latitude, ς is the sun zenith angle (Stull, 1995).

Solar flux – the flow of solar energy (Goudie, 1988).

Solar spectrum – the dark lines constituting the absorption spectrum exhibited by sunlight. The dark lines will appear when the radiation that passes trough the atmosphere is absorbed by cool gases in certain spectrums. This results in some blocked out, dark lines in the continuous spectrum. The dark lines are also called Fraunhofer lines (Considine, 1989).

Sun zenith angle, ς – defined as (C/4 - Ψ), where C=360° and Ψ is the local elevation angle of the sun above the local horizon (depends on latitude and longitude) (Stull, 1995).

Variance – the variance of a population is the average of the squares of the means [kolla upp]. Often used as a measure of dispersion (Considine, 1989).

Variance-covariance matrix – Used for expressing the covariance, the diagonal elements in the matrix are the variances and those off the main diagonal are the covariance values (CGCC glossary).

WAI - Woody Area Index, this is the area index of canopy woody components (Kucharik *et al.*, 1998).

α - Ratio of total woody area index to total plant area index (Kucharik *et al.*, 1998).

Ω - non randomness correction factor for leaves and branches (Kucharik *et al.*, 1998).

Table of contents

1. Introduction

Leaf area index, or LAI as the parameter is notated, is defined as one-half the surface area of leaves per unit ground surface [m^2/m^2] (Kucharik *et al.*, 1998). Because green leaves control many biological and physical processes in plant canopies, LAI is a very important parameter in terrestrial ecosystems (Chen *et al.*, 1997). LAI is for example the most important parameter for determining the growth and yield for crops (Goel and Thompson *et al.*, 1984). LAI is also important for estimating net primary production (NPP) and biomass on a global scale (Badhwar *et al.*, 1986).

One major problem is how to measure and estimate LAI. The measuring methods can be divided into two categories: direct measurements and indirect measurements. The direct measurements include harvest, leaf litter fall and applications of allometric equations [förklaring] to collection diameter data (Gower et al., 1999). The indirect measurements do not involve any destructive measurements. Instead different commercial products are used which, all measure the light transmittance through the canopy. (Gower et al., 1999). One example of such an instrument is the Li-Cor LAI-2000. The instrument however measures not just the leaf area but also the wood area. The measurements conducted with the LAI-2000 are therefore not actual LAI values but some composite value of leaf and woody area (Kucharik *et al.*, 1998). When calculating LAI one assumes that the foliage is randomly distributed, which is not always the case in reality. The LAI-2000 measurements must therefore be recalculated. Both Chen *et al.* (1997) and Kucharik *et al.* (1998) have presented approaches for recalculation of the LAI-2000 measurements.

Both direct and indirect measurements are rather time consuming, and the area coverage is poor. It would therefore be advantageous if LAI could be estimated with remote sensing, especially with satellite images, which provide great area coverage to a relative low cost. One way of using satellite images for estimation of LAI is by the inversion of a so-called canopy reflectance model. Nilsson and Peterson (1991) presented such a model designed for forest canopies called “a forest canopy reflectance model”. A new version was presented by Kuusk and Nilsson (2000). The model simulates the radiative behaviour and the reflectance of the canopy, given a set of input parameters. The model's output is the canopy's reflectance for different wavelengths. Since LAI is one of the input parameters, the model can be inverted with the satellite reflectance as input and a value of LAI can be retrieved. To obtain correct values of LAI it is necessary to have an accurate set of input data. Since the model needs many input data, this is a rather big problem. Another problem is to obtain accurate reflectance values from the satellite image. This can be problematic due to the atmospheric influence; when a satellite receives a signal reflected by land or sea surfaces, the signal is affected by the presence of the atmosphere. The influence is strongest in the visible and near infrared spectrum. The main processes at work are aerosol scattering and gaseous absorption. The result will be a distortion of the satellite data. This is however not a problem if the analyst is only interested in visual comparison or relative brightness, but if real reflectance or radiance is needed (as in our case) the atmospheric influence has to be removed. There are several ways of doing this; the histogram minimal method, for example, is an often-used procedure (see theory chapter or Campbell, 1996). The most powerful and advanced technique is however the use of a physical atmosphere correction model, such as the 6S model (Campbell, 1996). Given a set of input data the model simulates the signals Sun-surface-sensor path and corrects the distortion caused by the atmosphere (see theory chapter or Vermote *et al.*, 1997b).

1.1. Chapter summary

Chapters 2 to 5 consist of theory aiming to give the reader background knowledge of our methodology and the material used in the study. Chapter 2 introduce the reader to the theory of canopy/foliage reflectance. Chapter 3 gives the theory behind the models simulating the behaviour of the radiation in the canopy. The chapter also deals with the technical and physical background of the model. Chapter 4 describes the atmospheric influence on satellite images and some different methods for its correction. A rather detailed description is given of the atmospheric correction model 6S, the one we have been using in this study. Chapter 5 describes the Li-Cor LAI-2000, which is the instrument we have been using for estimating LAI and BAI. In chapter 6, basic theory of geometric and radiometric correction of a satellite image is given.

The methods, data and material that we have used in the study are presented in chapter 7. We have decided to list the in-parameters to the forest model and how they were estimated and acquisitioned. We also describe how the sensitivity analysis was performed.

All of the results are presented in chapter 8, and the discussion and conclusions are presented in chapter 9.

1.2. Aim

The main aim of this thesis is to investigate the possibility of estimating LAI with optical modeling and remote sensing in deciduous forest collections in southern Sweden.

Three objectives are constructed:

- To perform a correction for the atmospheric influence on a Landsat 7 ETM+ scene with the atmosphere correction model 6S.
- A sensitivity analysis of the forest model is performed to evaluate the influence of different input parameters on the calculated reflectance.
- Comparison between the modelled reflectance and the atmospherically corrected satellite reflectance to see if there exists any relation.

2. Theory of foliage reflectance

2.1. Leaf reflectance

The reflectance from a leaf is determined by the leaf structure as well as the biochemical constituents of the leaf. To understand the optical properties of a leaf, studies at a detailed level must be undertaken, see figure 1.

A leaf consists of several different layers with diverse optical functions. The uppermost layer, the epidermis, consists of cells fitted closely together. The other side of the leaf consists of the lower epidermis that has openings in the cell layer called stomata, which allow an exchange of water and carbon dioxide with the atmosphere. A wax layer called the cuticle covers the upper cell layer. Below the upper epidermis is the palisade layer that consists of cells rich in chlorophyll. The chlorophyll is situated in elongated cells called chloroplasts along with other pigmentation molecules. These cells are positioned vertically in the palisade layer. Below the palisade layer is the spongy mesophyll tissue. It consists of irregularly shaped cells separated by connected spaces. This gives the tissue a very large surface area. Leaf structure is not identical for all plants but this description gives a general idea of the major elements common to most species.

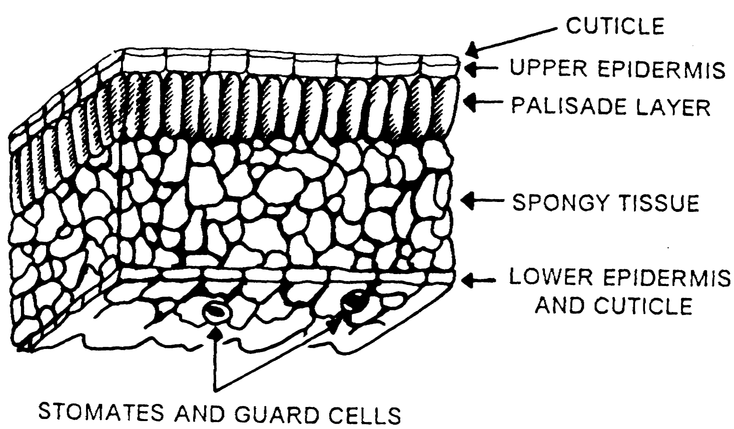

Figure 1. Cross section of a typical leaf (Campbell, 1996).

In the visible region of the spectrum the chlorophyll content controls the optical properties of the leaves. The chlorophyll absorbs the sunlight that makes photosynthesis possible and is most active in the blue and red region. Here, as much as 70% to 90% of the incident radiation can be absorbed. In the green region, the absorption is lower which allows a large portion of the green light to be reflected. This is why leaves appear green to the human eye.

In the near infrared spectrum the leaf reflectance is controlled by the structure of the spongy mesophyll tissue. The cuticle and epidermis are nearly completely transparent to the infrared radiation. Radiation passing through the upper epidermis is strongly scattered by the mesophyll tissue and the cavities. Very little radiation is absorbed and most is scattered upwards (reflected) and the rest is scattered downwards (transmitted). As illustrated in figure 2 the reflectance in the NIR region is greater than the reflectance in the visible region. Differences in reflective properties of plant species is more pronounced here than in the visible region (Campbell, 1996).

In the longer infrared wavelengths (beyond 1300 nm), leaf water content appears to control the spectral properties of the leaf. The term equivalent water thickness has been proposed to designate the thickness of a film of water that can account for the absorption spectrum of leaf at 1400 nm to 2500 nm. However, results from Gao and Goetz (1995) indicates that it is not only water content that is responsible for the optical properties in this spectra but also, to some extent, the content of lignin.

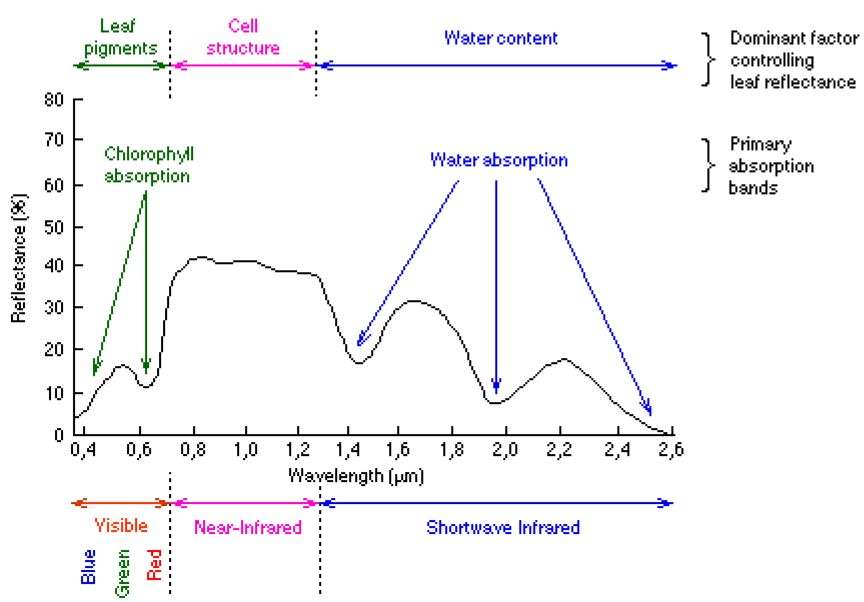

Figure 2. Typical spectral response characteristics of green vegetation (UCL department of Geography Staff Homepages).

2.2. Canopy reflectance

In the field, a vegetation canopy is composed of many layers of leaves, branches, stems and under story vegetation. Each of these components has many variables and therefore the reflectance from a canopy varies considerable from the reflectance of a single leaf. Leaves may vary in size and orientation, which leads to shadowing of various canopy elements, such as leaf, soil and under story vegetation. This decreases the reflectance below the values measured from single leaves, see table 1. However, the relative decrease is much lower in the NIR region than in the visible region. This is due to the optical properties of leaves in the NIR region.

Table 1. Single leaf and canopy reflectance (from Campbell, 1996).

	Percent Reflected	
	Visible	Near infrared
Single leaf	10%	50%
Canopy	3 – 5%	35%

The part of the radiation that is transmitted in the top layer of leaves is re-scattered on the next layer and transmitted back through the first layer. Therefore, infrared radiation is transmitted back through the upper leaves, resulting in a high reflectance (Campbell 1996), see figure 3.

Other factors affecting the reflectance from a surface are the view angle and the illumination angle (Deering, 1989). The effect of reflectance variation due to changes of these variables is described by the bi-directional reflectance distribution function (BRDF).

The forest reflectance model takes all of the above variables into account when calculating the reflectance from a forest collection i.e. it calculates the BRDF in specified view and illumination angles.

The BRDF often yields a peak of reflectance if the source of illumination (the sun) is directly behind

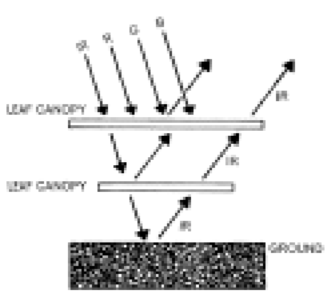

Figure 3. simplified illustration of behaviour of energy interacting with canopy. In NIR radiation transmitted through the top layer is available for reflection from lower layers (Campbell, 1996).

the sensor. This peak in reflectance is called ”the hot spot”. A typical BRDF is illustrated in figure 4 where the hot spot is visualised in increased reflectance right part of the figure. It occurs as only illuminated parts of an object is view by the sensor.

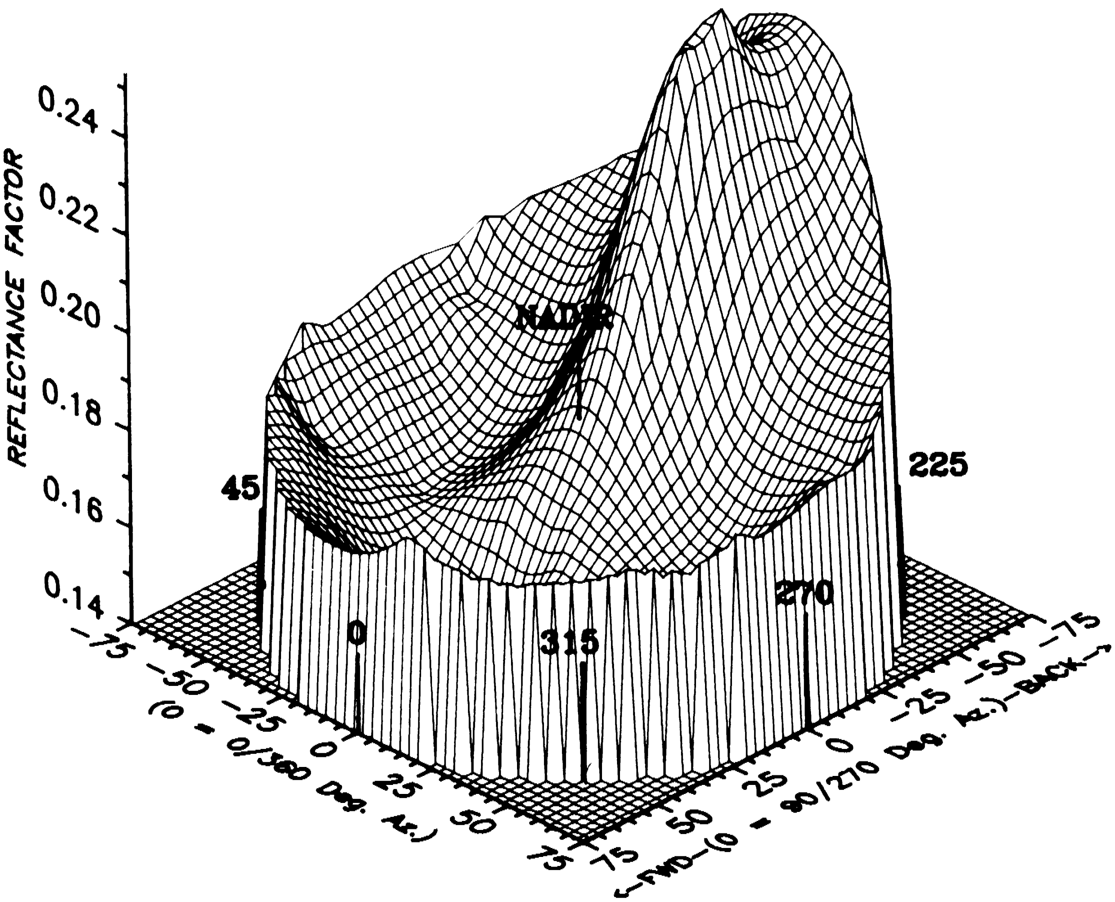

Figure 4. Oak-rangeland community bi-directional reflectance surface for 826 nm (Deering, 1989).

3. Model theory

3.1. The Forest Reflectance model

The forest model calculates the BRDF of a forest canopy from 400 nm to 2500 nm. Different size or species classes are possible as input to the model. Within each class, trees are considered identical. The reflectance can be calculated for any view direction and several view angles are possible when inverting the model. The model is thoroughly described in Nilsson (1990), Nilsson and Peterson (1991) and Kuusk and Nilsson (2000).

The forest model is a radiative transfer model i.e. it describes the radiative transfer within the canopy by numerical ray tracing or Monte Carlo methods. Radiative transfer models are capable of handling spatially heterogeneous canopies and can calculate the BRDF of the surface. They are very computationally expensive and often a large number of input parameters are required. Due to the complex computations of ray tracing or Monte Carlo simulations approximations are sometimes used. The forest reflectance model by Kuusk and Nilsson (2000) uses a two-stream approximation. Models using two-stream approximations define only two directions for the radiation: a hemispherically integrated upward direction and a hemispherically integrated downward direction. This simplification allows the upward and downward fluxes of radiation to be described by two differential equations that can be solved analytically (Sellers, 1989).

The forest model uses several sub models to calculate the reflectance from a forest collection. The Prospect model by Jacquemoud and Baret (1990), and improved by Jacquemoud et al. (1996) is used to calculate the optical properties of the leaves. The model is a radiative transfer model using a minimum of parameters including chlorophyll, protein, cellulose and lignin content and water thickness to calculate the leaf reflectance and transmittance in 400 to 2500 nm. In the visible part of the spectrum absorption is a function of pigment concentration such as chlorophyll a and chlorophyll b while in the NIR area the optical properties are modelled by the leaf structural parameter. In the longer wavelengths water is responsible for the optical properties of a leaf (Jaquemoud and Baret 1990, Jaquemoud *et al* 1996). The model assumes uniform distribution of water and pigment concentration in the leaf. It also assumes a constant surface roughness which may not the case. According to Jaquemoud and Baret (1990) these assumptions limits the accuracy of the model.

The MCRM (Multispectral Canopy Reflectance Model) model, developed by Kuusk (1995) at Tartu observatory in Estonia calculates the reflectance from the under story vegetation from parameters as ground LAI, leaf size, leaf angle distribution and the weights of Price's function for soil reflectance. The spectral distribution of soil reflectance depends on a very large number of parameters. Price (1990) describes the soil spectra using four functions. These functions reduce the number of input parameters to two parameters, with the ability to describe 94 % of the soil spectrum variance. The MCRM model also uses the Prospect model to compute the reflectance properties of the under story vegetation.

The 6S model (described below) is used to calculate the incident radiation flux. Input parameters to this sub model are the percentage of four aerosol components and aerosol optical thickness at 550 nm, see chapter 7.2.

3.1.1. Description of the model

The model represents the reflectance factor of a forest canopy R as the sum of four components:

$$R = R_{CR}^{1} + R_{GR}^{1} + R_{CR}^{M} + R_{GR}^{M} \qquad (1)$$

Where:

R^1_{CR} = single scattering from tree story crowns

R^1_{GR} = single scattering from ground vegetation and soil

R^M_{CR} = multiple scattering from tree story crowns

R^M_{GR} = multiple scattering from ground vegetation and soil

Tree crowns are modelled as semitransparent simple geometrical shapes such as ellipsoids and cones. Within each class, all trees are considered identical to the input parameters. The different components of equation 1 are calculated as follows:

R1cr: The single scattering inside a tree crown is the part of the reflectance caused by photons scattered once on a crown element.

$$R_{CR}^{1} = \frac{I_0 \mu_L \Gamma(r_1, r_2)}{\pi} \int V p_{00i}(r_1, r_2, s_1, s_2, \alpha) dxdydz \qquad (2)$$

Where:

I_0 = the incident radiation

μ_L = the density of LAI and BAI

Γ(r1, r2)/ π = area scattering phase function, a function that describes the angular distribution of the energy scattered, assumed to be bi-lambertian (described by Ross (1981) and Myneni (1989))

V = volume of a tree crown

$p_{00i}(r_1,r_2,s_1,s_2,\alpha)$ = the bi-directional gap probability inside the crown in direction r1 and r2, s1 and s2 are the distances to the crown perimeter and V is the crown volume

r1, r2 = directions towards the sun and the sensor

s1, s2 = the distance within the crown in directions r1 and r2 respectively. In figure 8 this coincides with the distance between M-M_1 and M-M_2.

R^1_{GR}: This is the radiation reflected directly on the ground vegetation or soil surface without interception from any part of a tree. It is calculated by:

$$R_{GR}^{1} = \rho(\vartheta_0, \vartheta) p(\vartheta_0, \vartheta) \qquad (3)$$

Where:

$\rho_{GR}(\vartheta_0,\vartheta)$=reflectance properties of ground surface in directions ϑ_0,ϑ

$p_{GR}(\vartheta_0,\vartheta)$=the bi-directional gap probability at ground level in directions ϑ_0,ϑ

The reflectance for ground vegetation and soil is a product of the reflectance properties of the surface calculated by the MCRM sub model and the bi-directional gap probability.

Multiple scattering is the reflection due to photons scattered at least twice by tree-crown, ground vegetation or the soil with the last scatter at a leaf in the case of R^M_{CR} and the ground vegetation or soil in the case of R^M_{GR}. The reflectance is calculated by the radiative transfer equation for homogenous canopies described by Ross (1981) and Nilsson (1991) and the two-stream approximation of radiative transfer equations is described by Sellers (1989). This means that the equation simulates the canopy with homogenously distributed plant material in the horizontal layer. From the transfer equation, canopy albedo A_M of multiple scattering and total downward flux F_{1M} are determined. Both are functions of solar zenith angle ϑ_0, total tree story foliage area index, foliage reflection and transmission and ground vegetation and soil albedo.

R^M_{CR}: The multiple scattering from tree crowns is calculated by:

$$R_{CR}^{M}(\vartheta_0, \vartheta) = A_M(\vartheta_0) A_M(\vartheta) / c_1 \qquad (4)$$

Where:

$A_M(\vartheta_0)$= the canopy albedo in the solar zenith direction ϑ_0

$A_M(\vartheta)$= the canopy albedo in the direction ϑ

c_1= normalizing constant

A_M is a function of solar zenith angle ϑ_0, LAI, BAI, optical properties of the foliage and ground albedo. A two stream approximation is used to speed up computations. According to Sellers (1989) this approximation yields an acceptable description scattering processes. For further reading Myneni *et al.* (1989) and Sellers (1989) is recommended.

R^M_{GR}: Multiple scattering from ground vegetation and soil is calculated by:

$$R_{GR}^{M}(\vartheta_0, \vartheta) = F_{1M}(\vartheta_0) F_{1M}(\vartheta) \rho_{GR}(\vartheta, \vartheta_0) a(0, \vartheta) a(0, \vartheta_0) / c_2 \qquad (5)$$

Where:

$F_{1M}(\vartheta_0)$= total downward flux at the ground level in the solar zenith direction ϑ_0.

$F_{1M}(\vartheta)$= total downward flux at the ground level in the direction ϑ.

$\rho_{GR}(\vartheta,\vartheta_0)$= the reflectance value of ground vegetation or soil in sun and view angle ϑ_0 & ϑ.

$a(0,\vartheta_0)a(0,\vartheta)$= the proportion of gaps in the forest canopy at ground level.

c_2 = normalizing constant

The bi-directional gap probability is a central part throughout the model. As the model divides a crown into small volume elements the bi-directional probability of free line-of-sight in solar and view direction is calculated for each element e.g. point M in figure 8. The bi-directional gap probability p_{00i} is actually a product of two independent probabilities,

$$p_{00i} = p_{1i} p_{2i} \qquad (6)$$

Where:

p_{1i} = the within-crown bi-directional gap probability

p_{2i} = the between-crown bi-directional gap probability

The within-crown bi-directional gap probability is calculated by:

$$p_{1i} = \exp(-\tau_{i1} l_{i1}) \exp(-\tau_{i2} l_{i2}) C_{HSI}(\alpha) \qquad (7)$$

Where:

τ_{i1} and τ_{i2} = the radiation extinction coefficient(m^{-1}) which is a function of leaf area index, branch area index and crown volume of the *i*th tree class.

l_{1i}, l_{2i} = the radiation path length within the crown. In figure 8 this coincides with M-M_1 and M-M_2.

$C_{HSI}(\alpha)$= the hot spot correction factor with α being the angle between view and solar direction, see Kuusk and Nilson (2000) for further reading.

This means that when crown density increases, i.e. leaf and branch area index increases and crown volume decreases, p_{1i} decreases, as shown in figure 5.

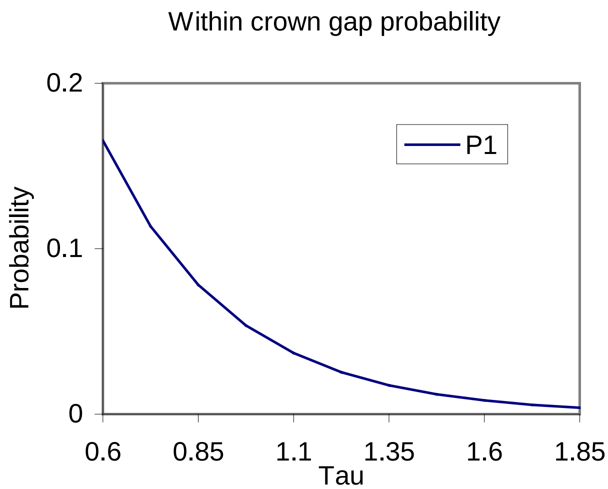

Figure 5. Within crown probability as a function of Tau. Tau is a function of Crown density, i.e. of LAI, BAI and volume. As the density increases, Tau decreases. Estimated values used for demonstration.

The between-crown gap probability is the part of the line-of-sight that lies outside the crown of interest, i.e. from the point M_1 to the upper part of the canopy in the view direction and from M_2 in the solar direction in figure 8. The between-crown gap probability is calculated by:

$$p_2 = \exp\left\{\Sigma_j \lambda_j b_{1j}(z,\vartheta)\left[S_{crown,j}(z,\vartheta) + S_{trunk,j}(z,\vartheta)\right]\right\} \qquad (8)$$

Where

λ_j= number of trees in class j per m^2.

$S_{crownj}(z,\vartheta)$ = the area of crown projection for class j at level z and direction ϑ.

$S_{trunkj}(z,\vartheta)$ = the area of trunk projection for class j at level z and direction ϑ.

$b_{1j}(z,\vartheta)$ = a function of gap probability in the crowns of class j, which depends on LAI and BAI similar to equation 7, as well as a grouping / regularity coefficient of the collection.

The equation assumes binominal distribution of trees. This means that the between crown gap probability is strongly affected by the crown radius and collection density. This is illustrated in figure 5 and 6, which are constructed from estimated values only.

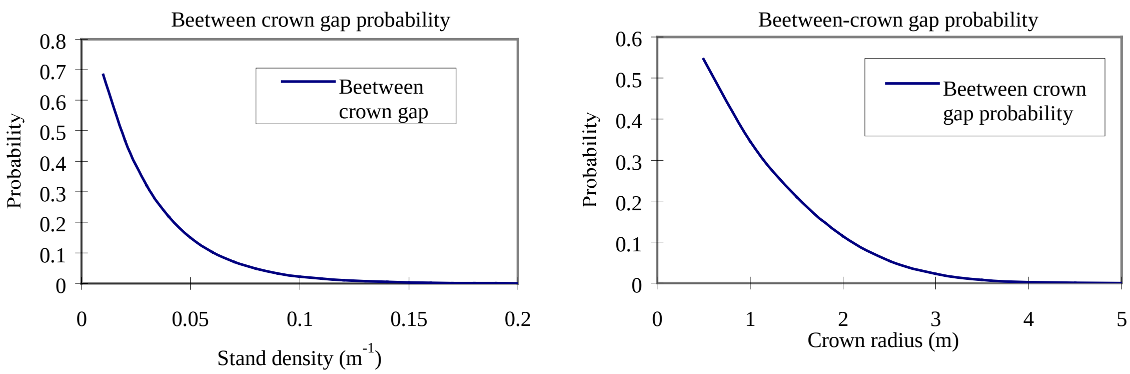

Figure 6 & 7. These figures are constructed by estimated values to illustrate how the between crown bi-directional probability may vary with different crown radius or collection density.

The independent components of the model, i.e. equation 2-5, are calculated for each specified wavelength and summarized by equation 1.

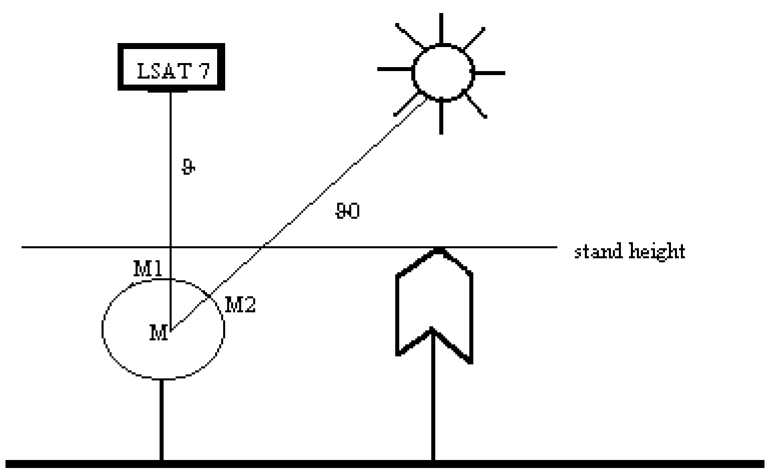

Figure 8. Simplified description the radiation paths in forest canopy reflectance as described by the model.

4. The atmospheric influence and its correction

Solar radiation travels through the atmosphere to the surface of the Earth, where it is reflected up to the satellite sensor in space. The signal received by the sensor would depend only on the surface reflectance in an ideal case: the illuminated surface would absorb some of the radiation and the rest would be directly reflected back into space. In reality, the signal depends on two atmospheric processes besides the surface reflectance. These are the gaseous absorption and the scattering of molecules and aerosols. The absorption and the scattering will result in loss of the surface reflected photons on their way to the sensor, typically 20% at 0.85μm and 50% at 0.45μm (Vermote *et al.*, 1997a). In other words, the surface will seem less reflecting.

For further understanding of the atmospheric influence, let's have closer look at the photons' path from the sun to the sensor.

In the Sun-surface path, some of the photons will be backscattered to space by molecules and aerosols. Most of these will not reach the surface and therefore not carry any information about the target, and the signal is said to be an interference term (Vermote *et al.*, 1997a). The photons not backscattered will reach the ground and illuminate it, either as direct or diffuse radiation.

At the ground, the photons are absorbed or reflected back into the atmosphere in a surface-sensor path. On this path, some of the photons will be scattered away from its path. On the other hand, some will be scattered towards the sensor. When trying to simulate the photons' way from the sun to the sensor one has to take this fraction in account. This is however problematic when dealing with non-uniform surfaces (Vermote *et al.*, 1997a). Photons can also be backscattered to the ground contributing to its illumination. This phenomenon is called the trapping effect. Although this phenomenon contributes to the illumination of the ground, when modelling the photons' path it can be neglected after one or two interactions (Vermote *et al.*, 1997a).

Accordingly, the atmosphere can have a big influence on the signal received by the satellite sensor. The atmospheric influence is not that great in airborne remote sensing, because the path through the atmosphere is shorter (although it can not be neglected).

Kaufman (1989) lists four ways (amongst many) in which the atmosphere can affect a satellite image:

- Because the atmospheric influence is wavelength dependent, it will modulate the brightness for each of the spectral bands. If one is to perform a classification based on brightness or "colour" the atmospheric influence has to be investigated and corrected for if the classification is to be correct. The changes in brightness can also affect the discrimination between stressed and unstressed vegetation. It has for example been shown that these influences can cause a delay of 3-7 days in detecting drought stress on wheat.
- The geometric resolution of the satellite image can be affected because of the atmospheric scattering that may alter the spatial distribution of reflected radiation from the target to the sensor.
- Because of the apparent brightness of the target, its albedo and reflectance may be affected.
- Sub pixel clouds may create some spatial variation in the apparent surface albedo.

4.1. Three kinds of atmospheric correction methods including a description of the 6S model

4.1.1. The histogram minimum method – HMM

Campbell (1996) suggests that the atmospheric correction methods fall into three categories. The simplest method is the one called the histogram minimum method (HMM). This procedure is based on examining the reflectance from objects with known brightness (the brightness recorded by satellite or airborne imagery). To achieve the best result using this method, the brightness of a target (man-made or natural) should be measured at ground level at the time of image acquisition. By comparing this brightness value of the target to the ones in the image the analyst can make a good estimate of the atmospheric influence. Campbell (1996) speaks of only one ground level measured target in the image. For the method to work properly more than one known target should be used, especially if sensors like Landsat TM or ETM are used with scenes covering an area of 185 ×185 km. In such a big area, the atmospheric influence is likely to vary. However, it would be very time consuming to measure the brightness of even one target. Therefore, the method is often reduced to finding the darkest object, often a large clear water body or shadows cast by clouds or other large features within the scene. These objects are chosen because they have a brightness of zero (or nearly zero) in the infrared portion of the spectrum. The reason for this is that clear water absorbs strongly in the infrared portion and that little energy is lost when the signal travels from shadowed pixels to the sensor. In a histogram of the brightness values, the pixels representing these dark areas should then be zero. If they are not, their values are assumed to indicate the atmospheric influence for each band. To correct for the influence these values are subtracted from all digital values in that band (Campbell, 1996).

The HMM is widely used method because of its simplicity and directness. One should have in mind that the method is approximate and have some major disadvantages. For example, the atmospheric influence does not affect all the pixels in a satellite image in the same way. The atmosphere can cause some pixels to be darker and some to be brighter, which has been shown in our own study (some pixels received a higher and some a lower reflectance value after the atmospheric correction, see appendix 1 and 2). This is due to the different atmospheric processes: a dark surface (surface reflectance > 0.05) will be mainly affected by scattering processes, while a bright surface (surface reflectance < 0.2) will be affected by atmospheric absorption (Kaufman, 1989). For remote sensing applications in arid regions the HMM can become impossible to use due to lack of clouds, shadows and large water bodies (Campbell, 1996). The HMM assumes that the brightness value of a large water body is zero (or very close to zero) in the infrared portion. However, due to alga bloom or influences from “bright” nearby land this may not be the case in reality (especially if a low spatial resolution sensor is used, such as the Landsat MSS).

4.1.2. Atmospheric correction by knowledge of interrelationships between spectral bands

This is the second category of the correction methods described by Campbell (1996). It is a more sophisticated method than the HMM. By examining the brightness of objects within the satellite image knowledge about the relationships between the spectral bands can be obtained. For example, values from each band can be paired with values from band 7 in a Landsat TM scene. A regression line can then be obtained and the *Y* intercept of the line used the correction value for the specific band. This technique can be extended by using a variance-covariance matrix; it is then called the covariance matrix method (CMM). These methods are not applied to the entire satellite image (as the HMM) but to local areas of 100-500 pixels (Campbell, 1996). Compared to the HMM, the generalization of the atmospheric influence is smaller. It does however assume that the land reflectivity is uniform for the specific region, which is not always the case. It is also a more time consuming method but, as Campbell (1996) puts it: “the procedure, if applied with care and with knowledge of the geographical setting, seems to be a robust and often satisfactory procedure”.

An example of this correction method is presented by Storvik (1986) who gives some methods for estimating parameters in a model based on a linearly structured covariance matrix.

4.1.3. Physically based atmospheric correction models

The last category described by Campbell (1996) is made up of models trying to model the physical behaviour of the photons on their sun-sensor path. By giving the (apparent) reflectance in one pixel, together with some other input parameters, the models calculate the real reflectance in the pixel (see appendixes for further specifications of input and output of the 6S model). Using these models is probably the best way to correct for atmospheric influences. The problem is that they are often very complex and needs a large set of input data.

The most known physical correction models are LOWTRAN, MODTRAN, 5S and 6S. They all use line-by-line computations of the atmospheric scattering and absorption for a variety of atmospheric conditions (Campbell, 1996; Kaufman, 1989; Vermote *et al.*, 1997b). The newest of the four models is 6S, the one we have been using in our study. Therefore the rest of this chapter is mainly devoted to this model.

The 5S model was developed in 1987 by Laboratoire d'Optique Atmospherique. The 5S stood for "Simulation of the Satellite Signal in the Solar Spectrum". The model worked well but it did have some limitations: it did not permit calculations of near-nadir (down-looking) observations, target elevation was not taken into account, it did not treat non-lambertian surface conditions, and the roles of CH4, N2O and CO was ignored (Vermote *et al.*, 1997b).

Because of these limitations, a new version was presented in 1997, ten years after 5S. The same scientists developed it and it was called 6S – "Second Simulation of the Satellite Signal in the Solar Spectrum". This new version was more powerful; it could handle all of the above-mentioned limitations; the computational accuracy for Rayleigh and aerosol scattering effects was improved; and the step-size or resolution for used spectral integration was improved to 2.5nm (5S had resolution of 5nm). There are though nevertheless still some limitations with 6S, for example it cannot handle spherical atmosphere (Vermote *et al.*, 1997b). For a complete description of the impact of the improvements between 5S and 6S, see Vermote *et al.* (1997b).

For an atmospheric correction model such as 6S to work it must be able to compute the gaseous absorption. In the solar spectrum the gases responsible for the absorption is oxygen (O_2), water vapour (H_2O), ozone (O_3), carbon dioxide (CO_2), methane (CH_4) and nitrous oxide (N_2O). The two most important gases are water vapour and ozone, these are assumed to different concentrations depending on time and location (the others are assumed to have constant concentrations throughout the atmosphere). Water vapour, for example, is located in the first 4 km of the atmosphere and is therefore highly dependent of the altitude up to 4 km (Vermote *et al.*, 1997b). Then it is very important to know how the different gases absorb and where in the solar spectrum the absorption takes place. When this is known its is possible to compute the exact absorption using line-by-line integration. In 6S, a spectral interval of 10 cm^{-1} is used (Vermote *et al.*, 1997a). After analysing the results one can see in which bands the absorbing effects are small, these are called atmospheric windows. The windows for satellites observations summarized by Vermote *et al.* (1997a) are as follows: between 0.40 and 0.75 μm in the visible and at about 0.85, 1.06, 1.22, 1.60, 2.20 μm in the near and infrared spectrum. See Vermote *et al.*, (1997a) for a complete description of the calculations and the computer code.

The other major phenomenon that has to be dealt with is the scattering effects. There are two different kinds of cases: the first is a case of a Lambertian uniform target (uniform surface reflectance), and the other a case where the surface reflectance is not uniform. In either case, it is most convenient to express the signal (received by the satellite) as a series of radiation interactions on its Sun-sensor path. In the case of a uniform surface reflectance the signal is treated in the following way (the following is taken from Vermote *et al.*, (1997a), who also summarize mathematical expressions):
Three steps/cases of surface illumination are being regarded.

- The direct downward solar flux that is being attenuated by the atmosphere on its way to the surface. It depends on the solar flux at the top of the atmosphere, the optical thickness and the sun zenith angle.

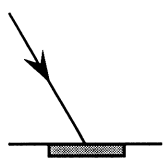

- The diffuse downward solar irradiance. It is noted by a diffuse transmittance factor that depends of the above-mentioned parameters. Because of the uniform surface, the factor is independent from the surface properties.

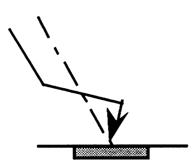

- Because of the trapping mechanism/effect a second scattered flux has to be regarded. It is depending on the target environment and on the “trapping reflections” between the surface and the atmosphere. The spherical albedo of the atmosphere is also taken into account.

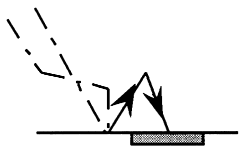

These three contributions make up the total illumination of the surface that now can be written as function of the total transmittance, the spherical albedo and the target reflectance.

The next step is to analyse where the radiance at satellite level results from. This is also depicted in three cases (from Vermote *et al.*, 1997a).

- The total solar radiance reflected by the surface directly transmitted to the sensor.

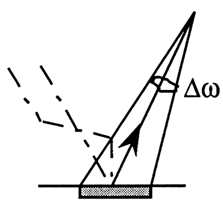

- The atmospheric radiance reflected to the sensor.

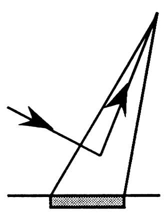

- The atmospheric diffuse transmittance. This is made up of the total downward flux reflected by the environment and the photons reaching the sensor by scattering.

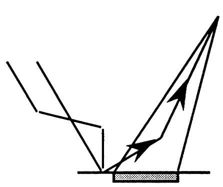

The apparent reflectance at the sensor can now be calculated. One should have in mind that this description is only valid for Lambertian surfaces. When dealing with a non-

Lambertian surface it gets a bit more complicated. The solution is to calculate a spatial average of the reflectance in each pixel over the whole target surface. This is said to be the environment reflectance, which is taken into account when calculating the apparent reflectance.

5. The Li-Cor LAI-2000

Direct destructive methods are used to estimate LAI. These are however rather expensive and time consuming and the output are point measurements that must be extrapolated to collection level (Chen et al, 1997). Another method to estimate LAI is litter fall collection, which can be used in deciduous forest with adequate spatial sampling technique. However, this method gives the maximum LAI during the growth period and not the actual LAI at an exact moment.

Indirect optical measurement methods are on the other hand a way to obtain quick and low-cost measurements over large areas. However all available instruments are limited by the complexity of canopy architecture in forest collections.

The Li-Cor LAI-2000 plant canopy analyser is commonly used to indirectly - measure LAI of various vegetation types. LAI can be derived from the probability that a beam of direct radiation will pass through a canopy. The penetration of a direct beam through any canopy is influenced by all of the canopy elements. The position, angle distribution and the spatial relations of the elements influence the extinction of solar radiation as it passes through a canopy (Norman and Jarvis, 1974; Welles 1990; Chen and Black, 1992; Smith *et al*., 1993). The basic concept is to use a model based on LAI and leaf angle distribution to describe radiation attenuation through a canopy. Measurements of radiation are made in or below the canopy and these are used to invert the model to estimate LAI. This approach requires leaves and branches to be randomly distributed throughout the collection (Kucharik *et al.*, 1998). The success of this approach is correlated to how well the radiation model describes the true canopy radiation properties.

In most natural forest collections, canopy elements are not randomly distributed. Non-randomness distribution of foliage can occur at leaf, branch and stem level. Radiation transmission through a canopy is greater for a clumped than a randomly distributed canopy. The assumption of random distribution of foliage may be valid for some closed canopies in deciduous forest, pastures, grasslands and agricultural crops, but it is invalid for open canopy forests such as boreal coniferous and aspen forests (Kucharik *et al.*, 1997, *Chen et al.*, 1997). Assuming a random distribution of foliage can produce errors of 100% or more (Gower *et al.*, 1999). The non-randomness factor is difficult to quantify and so far, the Li-Cor performs best in collections that close to random.

The instrument is active in the blue wavelengths (400-490 nm) in five independent sensors that measure in five zenith angles ranging from 0° to 70°. The calculation of LAI from these measurements are based on the probability of a direct beam penetrating the canopy at a zenith angle (Θ) described by:

$$P(\Theta) = \exp(-K(\Theta)L_t / \cos(\Theta) \qquad (9)$$

Where:

K(Θ)= the fraction of foliage projected in direction Θ (also referred to as the canopy extinction coefficient).

L_t= is the indirect measurement of LAI. However, this is not the actual LAI and is therefore called Plant Area Index (PAI).

L_t consists of all canopy foliage elements (leaves, branches, stem and a canopy non-randomness factor (Ω) and has therefore been referred to as effective LAI (Le). With multiple measurements of K(Θ) and L_t (one in each sensor and angle) simultaneously the model (eq. 9) can be inverted so that values of L_t can be obtained.

5.1. Obtaining LAI from Li-Cor LAI-2000 measurements

Measurements made in a forest collection are affected by leaves, branches, stem and the non-randomness factor so that the value of L_t is the PAI. To obtain the true LAI value from these measurements correct handling of BAI, stem and Ω is acquired. According to Kucharik *et al.* 1997 the woody part of the canopy must be deducted from the PAI. To accomplish this values of the Woody Area Index (WAI) and the non-randomness factor are needed. As shown by Chen et al (1997a) LAI is then estimated by:

$$LAI = \frac{(1-\alpha)*L_t}{\Omega}$$
$$\alpha = \frac{WAI}{PAI} \qquad (10,11)$$

This approach assumes that branches and stems are randomly located with respect to leafy foliage and that they are not preferentially shaded by leaves or shoots in the canopy (Kucharik *et al*. 1998).

However, Kucharik *et al.* (1998) proposes another approach, which involves the measurement of BAI by the MVI instrument. Since the LAI-2000 measures stem area in its quantity of L_t due to its wide field of view (0-70°) some quantity of the stem must be removed from the estimated LAI. In addition, the quantity of branch hemi-surface area in the crown must be accounted for. This is measured by the MVI or estimated from measured values from similar collections.

$$L = \left[(\frac{(L_e(\Theta) - \delta(f_L)B[\Omega_b(35)])\gamma_e}{\Omega_e(35)}) \right] - S \qquad (12)$$

where:

$Le(\Theta)$ = Measured value from LAI-2000

$\delta(f_L)$ = the fraction of the indirect branch hemi-surface area index that intercepts light in the canopy. This value is estimated from Kucharik *et al.* (1998).

γ_e = equals 1 for deciduous forests.

$B[\Omega_b(35)]$ = Branch area index measured by the MVI in zenith angle 35°.

$\Omega_e(35)$ = canopy leaf non-randomness factor at 35° zenith angle

These two approaches give very different results. The method presented by Chen (1997) yields lower values than the raw values from the LAI-2000 while the Kucharik (1998) approach yields somewhat higher values. We will calculate LAI with both methods and refer to them as LAI Chen and LAI Kucharik. We do not have access to the MVI instrument so we will use the values from our BAI measurements done with the LAI-

2000. This will result in errors but since the $B[\Omega_b(35)]$ term has such low weight (since it is multiplied by $\delta(f_L)=0.1$) the errors may be small.

5.2. Obtaining BAI from Li-Cor LAI-2000 measurements

By using the Li-Cor LAI-2000 in a forest collection where leaf-foliage is absent, the measured L_t consists only of the woody part of the canopy. Therefore, the effective Woody Area Index (WAI_e) is measured. Since the Li-Cor has a very large field of view, some of canopy measured consists of stems. To calculate BAI_e the stem contribution must be removed. It is necessary to have collection data on diameter, length and density of tree stems to estimate BAI_e by:

$$W_e=B_e+S \tag{13}$$

BAI_e consist of BAI*(a non-randomness factor). Kucharik *et al.*, (1998) suggests that this factor should be limited by Ω and 1 since branches are located close to leaves and shoots.

6. Geometric and radiometric correction theory

Satellite images are seldom delivered with a desired geometry. Therefore, a geometric correction has to be performed. The most widely used method is the so-called “geometric correction by resampling” (Campbell 1996). This method treats the satellite image as an array of values that must be manipulated in order to create a new array of values with the correct geometry. It can be symbolized as an array of pixel centres with a superimposed second array of pixel centres representing the transformed image with correct geometry (the output image). The relationship between the input and output image is established by the location of the GCPs – ground control points. GCPs are sites on the input satellite image that can be located with precision on the ground and on maps (Campbell, 1996).

When collecting the GCPs there exist some practical problems. The ideal GCP is as small as one pixel yet easily identified on the both input and output image. This is hardly the case in reality; the GCPs are often distinct areas consisting of a few pixels. Road intersections, stream junctions and water body edges are often used when collecting GCPs. The GCPs also have to be dispersed throughout the image if the correct geometry is to be obtained. The problem is that the GCP accuracy decreases with an increasing number of GCPs. A number of 16 GCPs with an accuracy of one third of a pixel is said to be reasonable. The GCP accuracy (the measure of the location error) is the root mean square error. This reports the standard deviation of differences (residuals) between actual values of GCPs and their calculated values (i.e., after registration) (Campbell, 1996).

When the GCPs are collected, the problem is how to best estimate the pixel values in the new corrected image arises. Three different approaches can be used for solving the problem. The first one is called the nearest-neighbour approach: each pixel receives its value from its nearest neighbour. The second is called bilinear interpolation; this approach is based on weighted average of the four nearest pixels. The third approach is called cubic convolution, which uses 16 pixels in the neighbourhood for a weighted average.

Another important pre-processing step, besides the geometric correction, is the process of converting the DN-values to reflectance. This process is called radiometric correction of the satellite image. The satellite image is handed to the analyst as a set of digital numbers (DN), consisting of series of bits. Because of each bit records an exponent of a power of 2 and each DN-value records 8 bits, the DN-values in a satellite image ranges from 0 to 255. The DN-values are also known as brightness values (BV), or digital counts. Sometimes the use of DN-values is satisfactory (for example when examine relative brightness or for visual comparison), but often the values must be converted to radiance or reflectance for further analysis. When performing this conversion information of the sensor calibration data must be known (Campbell, 1996). Therefore, different sensors use different equations for the radiometric correction. The equations used for radiometric correction of a Landsat ETM scene can be seen in the methodology chapter below or in the Landsat 7 Science Data Users Handbook available on the NASA homepage.

7. Data and methodology

The Landsat 7 scene was geometrically corrected to the digital version of Röda kartan so that the individual collections could be localized in the scene. A radiometric and atmospheric correction was performed according to the Landsat 7 Science Data Users Handbook and with the 6S model. Atmospheric data from SMHI was used as input data to the 6S-model. The positions of the forest collections were measured with DGPS. A center point and the boundaries for each collection were measured. Canopy structural parameters such as tree height, crown radius and LAI were measured in all collections.

The satellite reflectance at each collection center point was extracted from the Landsat 7 scene. A square of nine pixels was extracted with the center pixel being the collection center point. The mean of these nine reflectance values were calculated and used as the collection atmospherically corrected reflectance value.

A sensitivity analysis of the forest reflectance model was performed to investigate the influence of each parameter on calculated reflectance. Collection FT1 and SH5 were used as standard cases. Each parameter was changed ±20, ±40 and ±80 % from the standard case at a time while keeping the others fixed.

The reflectance from each forest collection were calculated using the field data, see table 2. The calculated reflectance was correlated against the extracted collection reflectance value.

Indices of satellite-measured reflectance were calculated for each collection. These indices were correlated against field measured LAI. The indices are calculated as:

$$NDVI = \frac{NIR - RED}{NIR + RED} \tag{14}$$

$$NIR / RED = \frac{NIR}{RED} \tag{15}$$

Indices are often used to estimate vegetation parameters from remotely sensed data (Asrar, 1989). However, the results have been poor and site or scene specific. It is therefore interesting to compare this method to the reflectance modeling approach.

7.1. Instruments and data

The instruments used in the study were:

- Differentiated GPS
- Li-Cor LAI-2000 (see theory chapter and manual for more information)
- Crown radius meter
- Diameter meter
- Suunto clinometer

The data used were:

- SMHI data set: SMHI provided an atmospheric data set, used for the atmospheric correction.
- LOPEX (Leaf Optical Properties EXperiment) 1993: The Lopex data set contains physical and biochemical data of more than 50 species of woody and herbaceous plants. It was developed by the Joint Research Institute at Ispra, Italy during the summer of 1993 for remote sensing applications. It has also served as a reference to develop the PROSPECT2 model. The biochemical constituents in the database are lignin, proteins, cellulose, starch, chlorophyll and water content (fresh weight – dry weight). The reflectance properties of each species are also included in the database. The collections of samples were done during two separate periods in the summer of 1993 close to the JRC in Italy, once in early summer and once in early spring. About 800g of leaves were collected for each sample. Five leaves were used for radiometric measurements such as reflectance and transmittance. Another five leaves were used to measure water content and the chlorophyll content. The rest of the sample were dried and shipped to two separate laboratories in France and Belgium where protein, cellulose, lignin, starch and carbon, hydrogen, oxygen and nitrogen were measured (Hosgood et al. 1995). Since the data is valid for Italian circumstances, the extrapolation to Swedish conditions is a possible source of errors.
- Landsat 7 ETM+ satellite image. The image covers most of Skåne. Its acquisition date was 990711.

- Digital and paper version of "Röda Kartan".
- Stanley 60 m open reel metric long tape.
- The Forest Reflectance Model (see theory chapter, Kuusk and Nilson, (2000) and Peterson and Nilsson, (1991) for more information).
- Multispectral Canopy Reflectance Model (Kuusk, 1994).
- The Prospect Leaf Optical Properties Model (Jacquemoud *et al*., 1996).
- The 6S Model. See theory chapter and Vermote *et al.* (1997a and 1997b) for more information.

7.2. Field measurements and study sites

When choosing the study sites, three criteria were to be fulfilled.

1. Due to the time limit, the sites were not be located more 50 km from Lund.
2. The sites had to represent different collection density, size and age.
3. The site had to be at least 50×50 m

We found ten sites. Five of them were located in Skarhult, which is nature reserve consisting of mainly cultivated deciduous forest such as oak, birch and beech. Two sites were located in Fulltofta, which is also a nature reserve. Fulltofta is a larger reserve then Skarhult with the main element being conifer forest. We were however able to find one beech and one oak collection. Two sites were located in Skrylle. Skrylle consists of mainly young, mixed forests. One site located in Torup, which is a reserve with many old deciduous collections. A collection name beginning with SH is located in Skarhult, FT in Fulltofta, S in Skrylle and T in Torup.

- SH1: A collection of dense beech with occasional birch. The collection is rather young.
- SH2: A full-grown mature oak collection with some beech. It consists of sparse tall trees (~30 m).
- SH4: A very sparse birch collection with dense grass, hazel bushes and raspberries constituting the understory vegetation. The birches are 12 to 16 m tall.

- SH5: A cultivated dense oak collection. The collection is fertilized which produces massive understory vegetation.
- SH6: A sparse and tall ash collection with large hazel plants. A very dense broad grass covers the ground.
- FT1: A full-grown tall beech collection (~30 m). The understory vegetation consists of raspberry and ferns.
- FT3: A mixed collection consisting of tall oaks (~25 m), smaller oaks (~18 m) and different bushes. Dense grass constitutes the understory vegetation.
- S4: Similar SH1 but without birch.
- S8: A mixed collection consisting of birch, beech, oak and mountain ash.
- T1: Similar to FT1 but with even taller trees. Rather large topographic differences.

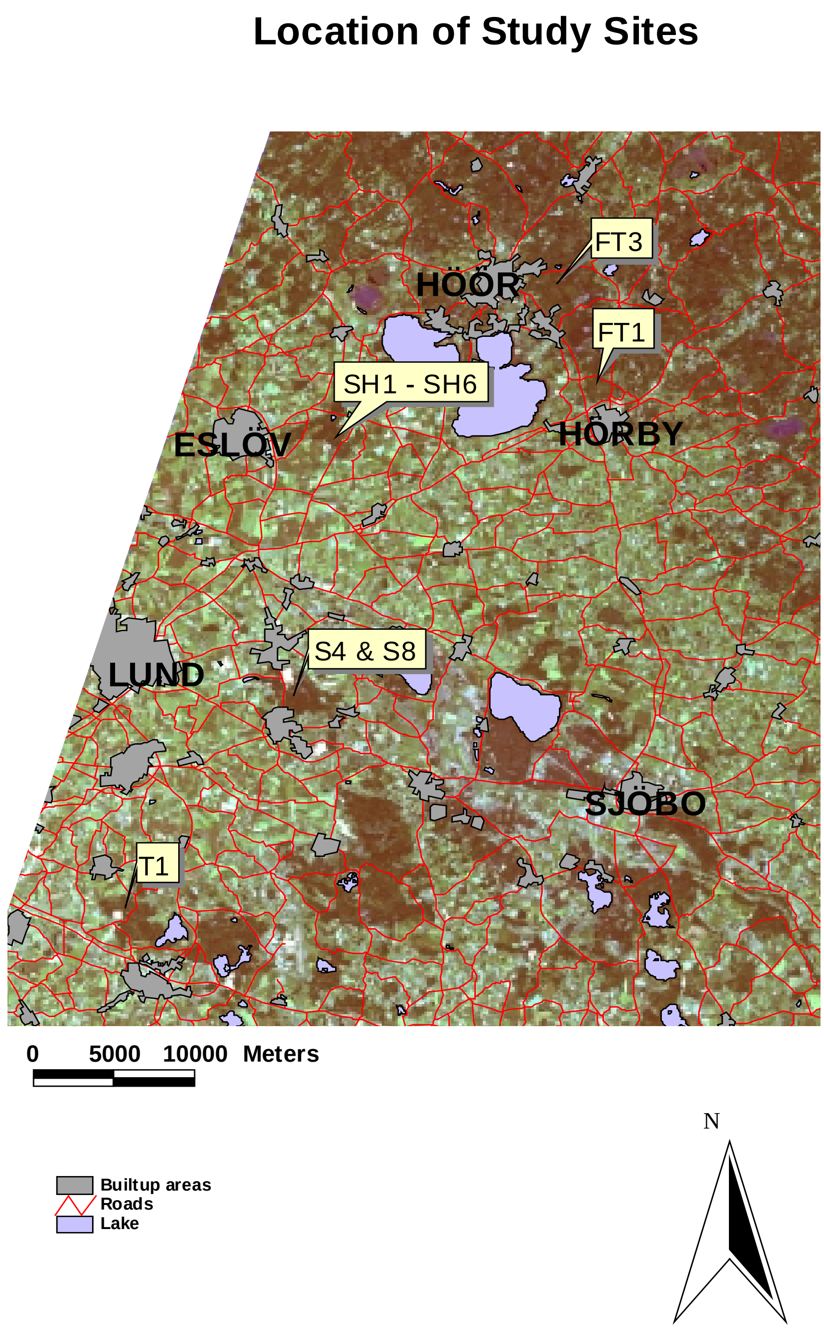

Figure 9. Location of study sites together with lakes, roads and builtup areas on the Landsat 7 false colour composite.

The fieldwork started in April (when no leafs were present) with Li-Cor measurements of BAI in Skarhult and Fulltofta (except for SH4, SH6, S4, S8 and T1 since these sites were added to the study at a later stage). When measuring, a transect was outlined in the area and at least 25 points were collected. It was important with a cloudy sky during the Li-Cor measurements if the values were to be correct. During the same time the position of the different sites were determined with a differentiated GPS. To be able to see how the LAI develops over time Li-Cor measurements were carried out again in May after the blossom period.

The rest of the fieldwork was carried out between 100700 and 210700 in Torup, Skrylle, Fulltofta and Skarhult. During this period tree height, crown inception, crown radius, DBH and collection density were measured. Because of the acquisition time of the satellite image (990711), the LAI measurements were collected during the corresponding period this year, 100700-120700. We measured the angle of the root, the crown inception and top of the crown with a Suunto. By measuring the angles from a fixed distance (usually 10 m) tree height and crown inception could be calculated. The crown radius was measured with an instrument (called in this study "crown radius meter") consisting of a mirror attached to a brass rod making it possible to determine the crown radius (we estimated that the crown radius on 20 m high tree could be obtained with an accuracy of 10 cm). When measuring the collection density a tree in the centre of the polygon was selected. This tree was then the centre of circle with a fixed radius in which all the trees were counted and measured. Number of trees divided by the circle area then gave the collection density. The trunk diameter at breast height (DBH) was measured with a diameter meter.

To obtain accurate values of LAI and BAI the LAI-2000 measurements had to be recalculated according to the approaches presented by Kucharik *et al.*, (1998) and Chen *et al.*, (1997).

7.3. Geometric and radiometric correction of the satellite image

In order to find our GPS points on our satellite image, it had to be re-projected to RT 90 (the Swedish coordinate system). We used the method described in the theory chapter. The satellite image was geometrically corrected to a digital version of Röda kartan. 12 GCPs were collected with a RMS error of less than one pixel. We used the nearest-neighbour approach for resampling of the pixels. The reason for this is that we did not want to alter the pixel values.

A radiometric correction of the satellite image had to be performed in order to obtain pixels reflectance values. The correction was performed according to the method described in the Landsat 7 Science Data Users Handbook. First, the DN-values were converted to radiance by the following equation.

$$\textit{(Spectral) Radiance} = \frac{(L_{\max} - L_{\min})DN}{255} + L_{\min} \qquad (16)$$

Where L_{min} and L_{max} are the spectral radiances for each Landsat 7 band (the L-values are enclosed with the image). The final step was to convert the radiance to reflectance by the following equation.

$$\rho_p = \frac{L_\lambda \cdot d^2 \cdot \pi}{ESUN_\lambda \cdot \cos\theta_s} \qquad (17)$$

Where ρ_p = Reflectance, L_λ = Spectral radiance (from equation 14), d = Earth-Sun distance in astronomical units (from Landsat 7 Science Data Users Handbook), $ESUN_\lambda$ = mean solar exoatmospheric irradiances (enclosed with the image), $\cos\theta_s$ = solar zenith angle (enclosed with the image).

7.4. Atmospheric correction scheme for the satellite image

The 6S model (see the 6S chapter and Vermote *et al.*, 1997a and 1997b for more information) was used for atmospheric correction of the satellite image. The correction was performed by following the scheme below.

First, the input data was calculated from an atmospheric data set provided by Thomas Person and Tomas Landelius from SMHI. The data set contained the β-value, the constant ozone value and water vapour content. The data were obtained 110799 – the same day, as our satellite image was acquisitioned. The β-value is the Ångström turbidity factor, which was used for calculation of the aerosol optical thickness (Kuusk, 1994). Although the constant ozone value was measured in Norrköping, it should, according to Thomas Person and Tomas Landelius, be representative for Lund because of the low spatial variation. The constant ozone value together with the water vapour content is used in the 6S model for description of the atmospheric conditions. No values could be obtained for the aerosol composition so we had to use a pre-defined aerosol model (aerosol type). Because our satellite image covers land areas adjacent to the sea we used the maritime aerosol model.

The radiometrically corrected reflectance values, extracted from our sites in the satellite image, were used as input. Because we were studying forests, we only corrected forest reflectance values. An example of an input file for the 6S model can be seen in appendix 1 (it can also be seen that we had to specify our own band limits).

6S then corrected the reflectance values for the atmospheric influence. Some of the values became higher after the correction, while others became lower. The reflectance values for channel 7 for example increased after the correction, while the values in channel 3 decreased. This can be seen in the box below, which is an extract from a 6S output file for channel 7. The complete file is presented in appendix 2. In the "result-box" below it can be seen that the input value is higher than the corrected value.

```
*******************************************************************************
*                        atmospheric correction result                        *
*                        -----------------------------                        *
*       input apparent reflectance            :    0.063                      *
*       measured radiance [w/m2/sr/mic]       :    1.291                      *
*       atmospherically corrected reflectance :    0.069                      *
*       coefficients xa xb xc                 :  0.05504  0.00190  0.01158    *
*       y=xa*(measured radiance)-xb;  acr=y/(1.+xc*y)                         *
*******************************************************************************
```

Figur 10. “Result-box” extracted from the 6S output file in appendix 2.

The correction resulted in linear equations between atmospheric corrected values and the input values. The equations can be seen in table 4 in Atmospheric correction results, chapter 8.1.

7.5. The model parameters

The parameters in the forest reflectance model had to be estimated as accurately possible in order to get a good result when performing the simulations. An example of an in-file can be seen in appendix 5. In the section below, a description of how the different parameters was obtained and estimated is presented. Only the most important parameters are presented.

- *Logical parameter of crown shape* (ellipsoid or cylinder + cone). Since we were studying, deciduous species ellipsoid crown shape was chosen.
- *Collection density*. Parameter measured in field.
- *Tree height*. Parameter measured in field.
- *Crown radius*. Parameter measured in field.
- *Length of the cylindrical part of the crown*. Parameter not used in simulation.
- *Crown radius*. Parameter measured in field.
- *DBH, trunk diameter at breast height*. Parameter measured in field.
- *LAI, leaf area index*. Parameter measured in field.
- *BAI, branch area index*. Parameter measured in field.

- *Grouping index*. We set the parameter to 1, which denotes a random collection. The parameter was sat to 1.1 for FT3 (a value >1 denotes a regular collection)
- *Shoot shading parameter*. When studying deciduous forests the shoot shading parameter should be set to one (Gower *et al.*, 1999).

7.5.1. PROSPECT model parameters

- *Chlorophyll content*. Calculated from the LOPEX data.
- *Protein content*. Calculated from the LOPEX data.
- *Lignin and cellulose content*. Calculated from the LOPEX data.
- *EWT, effective water thickness*. We set EWT to 0.0080 as suggested by Nilson (2000).
- *Leaf structure parameter, number of cell layers in a leaf*. Used 2.5 (Kuusk, 2000), Jaquemoud and Baret (1990) recommend values ranging from 1.5 – 2.5.
- *Refractive index ratio*. We have set the parameter to 1.37 as suggested by Kuusk (2000), Jaquemoud and Baret (1990) recommend values between from 1.3 – 1.5.

7.5.2. Canopy reflectance model parameters for ground vegetation

- *LAI for ground vegetation*. Using values from Nilson *et al*., (2000).
- *Leaf size parameter for ground vegetation*. Using values from Nilson *et al*., (2000).
- *Chlorophyll content for ground vegetation*. Using values from Nilson *et al*., (2000).
- *Weight of 1:st Price's vector*. Using values from Nilson *et al*., (2000).
- *Leaf size parameter, number of crown cells*. Using values from Nilson *et al*., (2000).

7.5.3. 6S model parameters

- *Aerosol model*. Using values provided by SMHI.
- *Visibility, optical depth*. Using values provided by SMHI.

7.5.4. MCRM parameters

- *PROSPECT parameter for ground vegetation (cW, cP, cC, N).* Using default values.
- *Parameter for soil reflectance model*. Using default values.
- *Number of sun angles and spectral channels*. Using one sun angle, number of spectral channels depending on spectral resolution.
- *Sun zenith angles*. Sun zenith angle=36° according to the information file enclosed with the satellite image.
- *Nadir- and azimuth angles*. Because we used a satellite image, the nadir- and the azimuth angle are zero.

Table 2. Shows the parameter values for the different sites.

Collection	Species	Density [#/m^2]	Height [m]	Crown Length [m]	Crown radius [m]	DBH [cm]	LAI Chen [m^2/m^2]	LAI Kucharik [m^2/m^2]	BAI [m^2/m^2]	Chlorophyll content [µg/cm^2]	Protein content [g/cm^2]	Lignin & Cellulose [g/cm^2]	Leaf N	Eq. water Thickness [cm]
FT1	beech	0.0095	29.13	18.01	5.05	57.77	1.78	2.64	0.81	44.8	0.0005	0.001	2.5	0.008
FT3A	oak h	0.0191	19.19	16.46	1.88	30.75	2.71	3.34	0.49	65.0	0.0010	0.003	2.5	0.008
	bush	0.0318	3.53	3.53	1.26	17.00				65.0	0.0010	0.003	2.5	0.008
SH1	beech	0.0300	15.95	13.05	2.35	20.50	3.44	4.30	0.76	44.8	0.0005	0.001	2.5	0.008
	beech	0.0300	4.94	3.35	0.95	4.50				44.8	0.0005	0.001	2.5	0.008
	birch	0.0100	25.80	19.43	2.25	23.50				45.0	0.0009	0.002	2.0	0.008
SH2	oak h	0.0059	29.40	18.00	3.40	50.97	2.38	3.09	0.63	65.0	0.0010	0.003	2.5	0.008
	beech	0.0147	24.00	17.66	4.10	40.00				44.8	0.0005	0.001	2.5	0.008
	beech	0.0059	16.96	14.75	2.38	14.00				44.8	0.0005	0.001	2.5	0.008
SH4	birch	0.0501	14.51	7.85	1.98	18.00	0.86	1.28	0.26	45.0	0.0009	0.002	2.0	0.008
SH5	oak	0.0500	17.28	12.04	2.21	22.75	2.89	3.58	0.54	65.0	0.0010	0.003	2.5	0.008
	oak	0.0400	5.40	4.03	1.19	6.75				65.0	0.0010	0.003	2.5	0.008
SH 6	ash	0.0159	30.21	18.89	2.39	26.25	1.88	2.54	0.52	75.0	0.0010	0.002	2.5	0.008
	ash	0.0095	7.13	3.83	1.59	10.75				75.0	0.0010	0.002	2.5	0.008
	hazel	0.0064	8.14	8.14	3.15	25.50				48.6	0.0010	0.001	2.5	0.008
T1	beech	0.0286	35.33	25.13	5.51	52.60	2.47	3.48	0.81	44.8	0.0005	0.001	2.5	0.008
S4	beech	0.0300	25.16	16.59	2.41	30.25	4.08	4.87	0.80	44.8	0.0005	0.001	2.5	0.008
	beech	0.0600	11.07	9.75	2.19	8.50				44.8	0.0005	0.001	2.5	0.008
S8	birch	0.0500	17.06	9.47	1.39	18.50	3.37	4.17	0.71	45.0	0.0009	0.002	2.0	0.008
	beech	0.0100	7.49	5.87	3.25	11.00				44.8	0.0005	0.001	2.5	0.008
	m. ash	0.0600	5.48	3.87	2.00	8.75				75.0	0.0010	0.002	2.5	0.008
	oak	0.0200	5.01	1.57	1.38	5.75				65.0	0.0010	0.003	2.5	0.008
	m. ash	0.0400	1.30	1.30	0.21	3.00				75.0	0.0010	0.002	2.5	0.008

7.6. Sensitivity analysis

A sensitivity analysis was performed in order to study the importance of the different parameters in the forest reflectance model. Using a standard case, FT1 and SH5, each parameter was varied ±20%, ±40%, ±80%, while the other parameters were fixed for these collections. Varying a parameter yields changes in calculated reflectance. The larger this change is, the more sensitive is the model to this parameter.

The reflectance obtained from the modelling with changed input data were divided with the reflectance from the standard case. The result can be shown in table 5 and 6 (only the ±20% variation is presented for all parameters). This analysis would show us how the importance of the different parameters in the forest reflectance model.

7.7. Reflectance modelling

The reflectance of each collection was modelled and compared to the satellite reflectance data. The model was run with the parameters in table 2. The LAI and BAI for each class were adjusted using equation 13 – 16. In the case of several size or species classes within a collection the measured LAI and BAI had to be divided between the classes. This was done based on the DBH – to- total DBH in each class weighed to the number of trees in a class. The LAI and BAI were then divided among the classes based on this ratio.

No actual measurement of the understory vegetation had been done so the values were taken from Nilson *et al.*, (2000). However, in field large differences in understory vegetation had been noticed so the literature-data was modified. According to Nilson *et al.*, (2000) understory LAI values for brad grasses is approximately 0.848; relative element size 0.1; chlorophyll content 34.9 and the first soil vector parameter 0.2878; leaf water thickness 0.008 cm; leaf protein content 0.0015 mg/cm^2; cellulose and lignin 0.008 mg/cm^2, effective number of leaf layers 1.7. Only 1.5, 2.0 and 2.5 modified the LAI.

Table 3: understory vegetation parameters. Sl is relative element size, CAB chlorophyll content and S1 the first soil vector parameter

Collection	LAI	Sl	CAB	S1
FT1	1.2	0.1	34.9	0.2878
FT3	0.848	0.1	34.9	0.2878
SH1	0.848	0.1	34.9	0.2878
SH2	0.848	0.1	34.9	0.2878
SH4	1.5	0.1	34.9	0.2878
SH5	2.12	0.1	34.9	0.2878
SH6	1.5	0.1	34.9	0.2878
Skrylle4	0.848	0.1	34.9	0.2878
Skrylle8	0.848	0.1	34.9	0.2878
Torup1	1.2	0.1	34.9	0.2878

7.7.1. Inversion of the model

The inversion of the model determines the model parameters from the measured reflectance. In the inversion, we use the structural parameters obtained by field measurements and presented in table 2. The leaf biochemical parameters are obtained from the LOPEX data set. The interesting parameter for inversion is LAI and it is supposed that if LAI is unknown BAI is unknown as well, thus LAI and BAI are free parameters.

The in data to the inversion model is as in the direct mode the structural, biochemical and understory vegetation parameters but also the reflectance measured by satellite or airborne sensors. Some parameters are held free and are computed within specified limits. Since the canopy reflectance is a non-linear function, a Merit-function is built by the model that has it’s minimum when the calculated reflectance values differs least from those measured. The merit function is dependent on the input parameters and serves as a measurement of the difference of calculated and measured reflectance (Kuusk, 1991).

A problem with the model inversion is that only the parameters of the first class can be obtained by inversion i.e. the parameters of the other classes of the collection must be known. Input data to the subclasses were taken from table 2.

8. Results

8.1. Atmospheric correction results

The atmospheric correction resulted in linear equations from which the reflectances could be calculated from the DN-values. The equations and R^2 are presented in table 4.

Table 4. The equations and the R^2 for the different channels.

Channel	Equation	R^2
ETM 1	Y = -1.3E-01 + 2.35E-03X	R-Sq = 98.7 %
ETM 2	Y = -5.8E-02 + 2.10E-03X	R-Sq = 99.8 %
ETM 3	Y = -0.0311 + 0.0017X	R-Sq = 99.0 %
ETM 4	Y = -3.4E-02 + 2.64E-03X	R-Sq = 99.8 %
ETM 5	Y = -2.1E-02 + 2.37E-03X	R-Sq = 100.0 %
ETM 7	Y = -2.1E-02 + 2.44E-03X	R-Sq = 100.0 %

8.2. Sensitivity analysis results

The results from the sensitivity analysis are summarized in tables 5 and 6. Although the sensitivity analysis was run on 20%, 40%, 80% differences only the 20% difference is summarized in table SA. Overall, the Crown radius is the most important parameter together with Chlorophyll content and Leaf structural parameter.

The deviations from the standard file have been divided into four different classes. The classes are divided as described below.

Blue: deviating ± >1% from the standard value.

Green: deviating ± 1 to >5% from the standard value.

Yellow: deviating ± 5 to >10% from the standard value.

Red: deviating ± ≤10 % from the standard value.

The parameters in the tables are listed so that the most depending parameter is placed first and the least depending placed last.

Table 5. Sensitivity analysis results for SH5.

		ETM1	ETM2	ETM3	ETM4	ETM5	ETM7
Crown	-20%	-9.55	-13.33	-9.55	-9.33	-13.38	-18.77
Radius	+20%	11.71	14.39	11.86	8.17	12.13	17.35
Leaf struc-	-20%	-15.18	-15.43	-14.56	-0.81	-2.88	-6.70
Ture para.	+20%	17.47	14.74	15.48	0.44	2.24	5.61
Chlorofyll	-20%	22.51	20.11	20.12	0.00	0.00	0.00
	+20%	-13.21	-14.21	-12.78	0.00	0.00	0.00
LAI	-20%	13.56	5.20	12.13	-2.50	0.14	2.23
	+20%	-10.27	-4.41	-9.28	1.70	-0.55	-2.28
Collection	-20%	-4.39	-6.68	-4.44	-3.34	-6.19	-9.77
Density	+20%	4.85	6.46	4.90	2.92	5.39	8.45
EWT	-20%	0.00	0.00	0.00	0.03	4.43	7.30
	+20%	0.00	0.00	0.00	-0.03	-4.00	-6.28
Ground	-20%	0.95	1.97	8.83	-5.10	-1.79	-0.07
Vegetation	+20%	-0.11	-0.69	-3.68	2.88	0.92	0.12
BAI	-20%	-4.70	-0.08	-3.63	2.52	0.82	-0.65
	+20%	4.61	0.10	3.55	-2.32	-0.77	0.60
Tree	-20%	0.85	0.79	0.89	1.75	2.01	3.44
Height	+20%	-0.09	-0.21	-0.12	-1.33	-1.57	-2.89
Crown	-20%	0.09	-0.42	0.10	-2.26	-1.54	-1.17
Length	+20%	0.43	0.73	0.38	2.59	1.74	1.26
Lignin and	-20%	0.11	0.21	0.12	1.38	1.83	3.57
cellulose	+20%	-0.09	-0.23	-0.12	-1.34	-1.75	-3.31
Protein	-20%	0.09	0.15	0.09	1.03	0.81	1.77
	+20%	-0.04	-0.18	-0.12	-1.01	-0.80	-1.70
DBH	-20%	0.29	0.23	0.25	1.10	0.61	0.23
	+20%	-0.22	-0.24	-0.24	-1.04	-0.58	-0.22

Table 6. Sensitivity analysis results for FT1.

		ETM1	ETM2	ETM3	ETM4	ETM5	ETM7
Crown Radius	-20%	-13.53	-13.66	-4.23	-14.51	-16.38	-19.78
	+20%	15.29	15.12	8.34	13.06	15.45	18.88
Leaf structure para.	-20%	-16.96	-12.08	-11.86	-2.23	-4.29	-7.30
	+20%	17.39	11.02	11.62	1.68	3.51	6.21
Chlorofyll	-20%	21.93	15.53	15.26	0.00	0.00	0.00
	+20%	-14.90	-11.83	-10.85	0.00	0.00	0.00
Collection Density	-20%	8.17	-5.00	-1.31	-4.60	-5.69	-7.29
	+20%	-5.55	9.59	4.23	7.80	9.90	12.68
LAI	-20%	6.76	2.29	8.01	-4.05	-0.58	0.69
	+20%	-5.53	-2.24	6.29	2.96	0.02	-1.08
EWT	-20%	0.00	0.00	0.00	0.03	5.83	7.97
	+20%	0.00	0.00	0.00	-0.03	-5.02	-6.74
Ground vegetation	-20%	0.44	0.86	3.52	-2.58	-1.14	-0.07
	+20%	-0.57	-1.20	-5.04	4.01	1.68	0.10
Tree Height	-20%	1.00	1.07	1.58	2.41	1.52	0.80
	+20%	-0.73	-0.82	-1.16	-2.24	-1.36	-0.68
BAI	-20%	-2.72	0.90	-1.20	3.57	0.78	-0.50
	+20%	2.49	-0.87	1.09	-3.30	-0.76	0.42
Crown Length	-20%	-0.07	-0.20	0.62	-1.46	-1.02	-0.80
	+20%	0.16	0.29	-0.43	1.60	1.09	0.83
Lignin and cellulose	-20%	0.07	0.14	0.07	0.62	0.71	1.78
	+20%	-0.08	-0.15	-0.07	-0.65	-0.75	-1.82
Protein	-20%	0.06	0.11	0.06	0.50	0.31	0.95
	+20%	-0.06	-0.11	-0.06	-0.49	-0.31	-0.93
DBH	-20%	0.26	0.31	0.43	0.91	0.55	0.27
	+20%	-0.21	-0.25	-0.35	-0.73	-0.44	-0.22

Visible region 450 - 700nm

In the visible region, the Chlorophyll content is the dominating factor together with the leaf structural parameter and crown radius followed by LAI and collection density which has moderate influence on the reflectance. Other parameters have negligible influence on the reflectance in this region.

NIR region 700-1600nm

In this region crown radius is the dominating parameter. The density and leaf structural parameter is has moderate influence on the reflectance in ETM4 but this increases in ETM5. LAI low to moderate influence in ETM4 but this weakens even more in ETM5.

The leaf biochemical properties low to no influence. Chlorophyll content has no influence at all in these wavelengths. The equivalent water thickness has very low influence in ETM4 but this increases in ETM5.

The MIR region 2090- nm

Here crown radius and density has a large influence on the reflectance. The leaf structural parameter and water thickness has also a large influence here. This increase of importance of the water thickness is also reported by Jacquemoud *et al*., 1995 and is due to the absorption of radiation from water at these wavelengths. The other parameters have low to very low influence.

Crown Radius

The crown radius has very large impact on the reflectance. As shown in figure 11 the influence is large throughout the spectra.

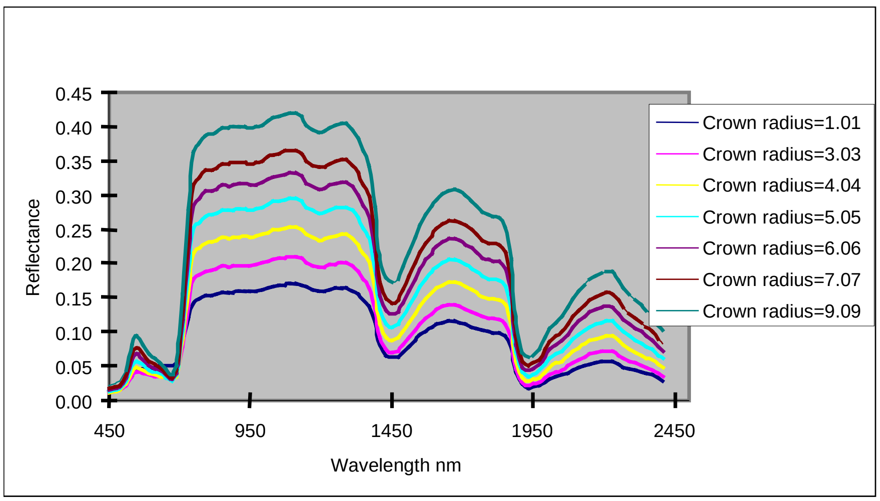

Figure 11. Reflectance variation due to changes in crown radius.

LAI

The LAI has a moderate influence on the reflectance. As shown in picture LAI and in table SA the model is most sensitive to LAI in ETM3 and ETM4. In ETM3 an increase in LAI induce a decrease in reflectance while in ETM4 an increase of LAI induces an increase of reflectance. Hence, the difference between ETM3 and ETM4 increases as LAI increases. The influence of LAI in ETM4 and ETM3 seems to decrease as LAI increases. As shown in figure 12, LAI there is a high sensitivity to LAI in ETM4 when LAI<2 - 2,5. When is higher than this the response in reflectance change is not as large as when LAI<2,5. This is also valid for ETM5 and 7 but the response is not as strong as in ETM4. In ETM3, the same break point can be found but there is a decrease in reflectance as LAI increases.

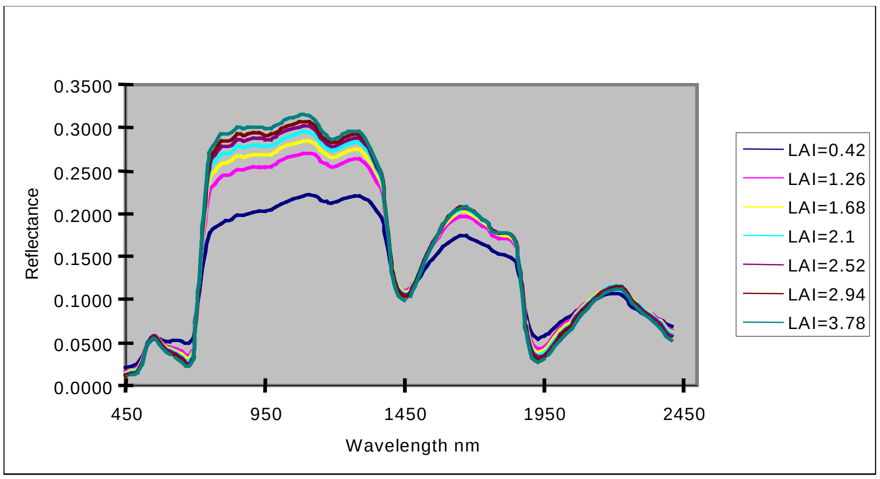

Figure 12. Reflectance variation due to changes in LAI.

Chlorophyll

The influence of chlorophyll is limited to the visible region as shown in figure 13. Here the influence is very strong.

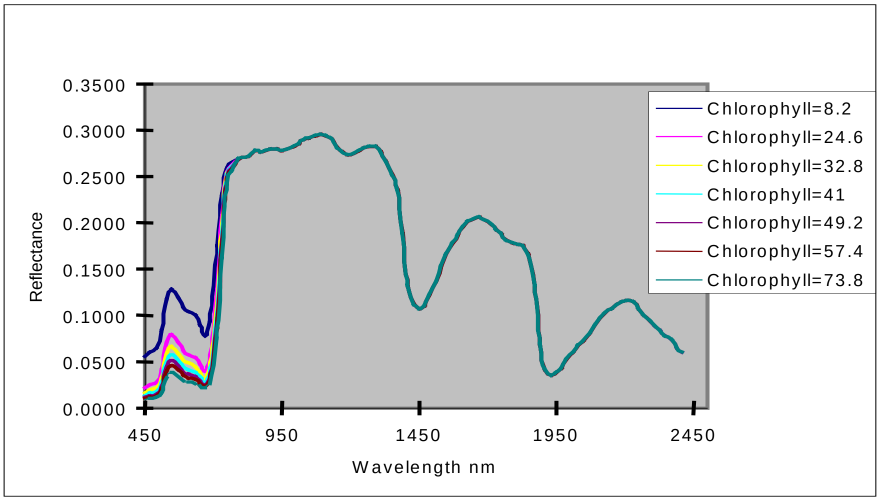

Figure 13. Reflectance variation due to changes in chlorophyll content.

Equivalent water thickness

The influence of water thickness is on the reflectance is absent in the visible region. In the NIR, it is very small but it increases, as the water absorption gets stronger in the longer wavelengths (see figure 14). This agrees with results reported by Jacquemoud et al. (1995) and Gao and Goetz (1995).

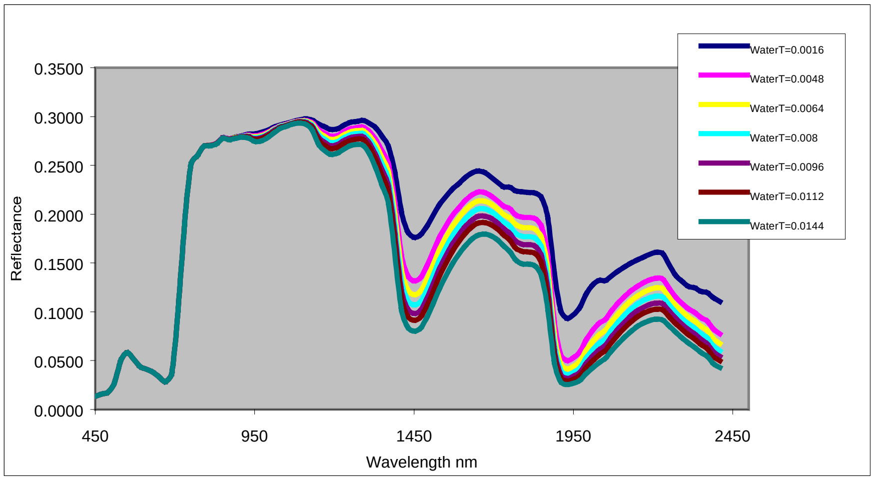

Figure 14. Reflectance variation due to changes in EWT.

Understory vegetation

The importance of understory vegetation can be strong depending on the canopy closure. Canopy closure is related to crown volume and crown density. When the canopy closure is low, i.e. a sparse collection or low crown radius or low crown density more of the understory is visible to the sensor. Hence increases the influence of the understory under these conditions. It is therefore important to have reliable understory vegetation data. As shown in tables 5 and 6 the influence of understory vegetation is low in the FT1 case but somewhat higher in the SH5 case. The strongest influence of the understory LAI is found in NIR, as can be seen in figure 15.

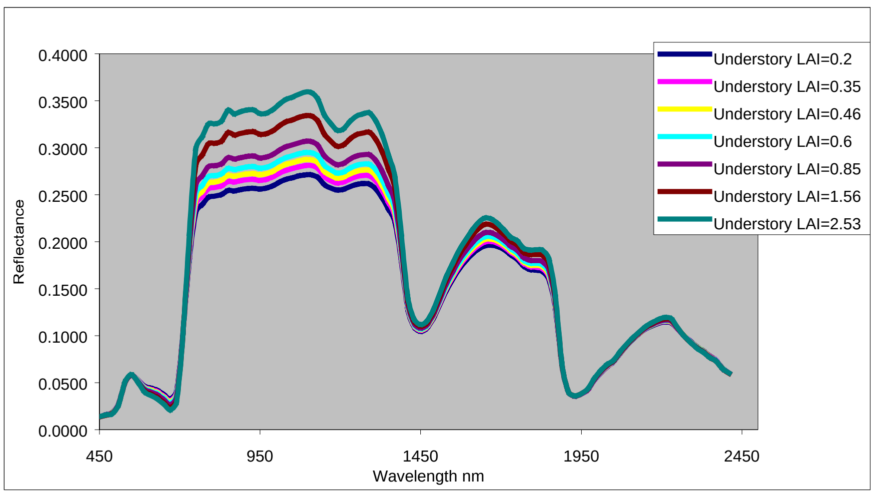

Figure 15. Reflectance variation due to changes in understory vegetation.

8.3. Reflectance modelling results

The modelled reflectance data where correlated against the satellite data in each Landsat 7 channel for both the simulation with LAI corrected with the Chen method and LAI corrected with the Kucharik method. The results are presented in table 7 and figure 16-27.

The correlation coefficient measures if there exists any linear relation between two variables, that is if it proper to express the relation linear (Körner and Wahlgren, 1993). The correlation coefficient ranges from –1 to 1, where 0 indicates no relationship. Low correlation coefficients were obtained with the best results in ETM5 and ETM3. The low values indicate that the model can't simulate the reflectance of our collections properly with the set of input data we have used.

Table 7. Correlation coefficients of satellite data and modelled reflectance data.

Channel	Chen Data (r)	Kucharik Data (r)
ETM1	0.27	0.20
ETM2	0.19	0.23
ETM3	0.44	0.21
ETM4	0.04	0.19
ETM5	0.55	0.58
ETM7	-0.22	-0.17

8.3.1. Chen corrected data

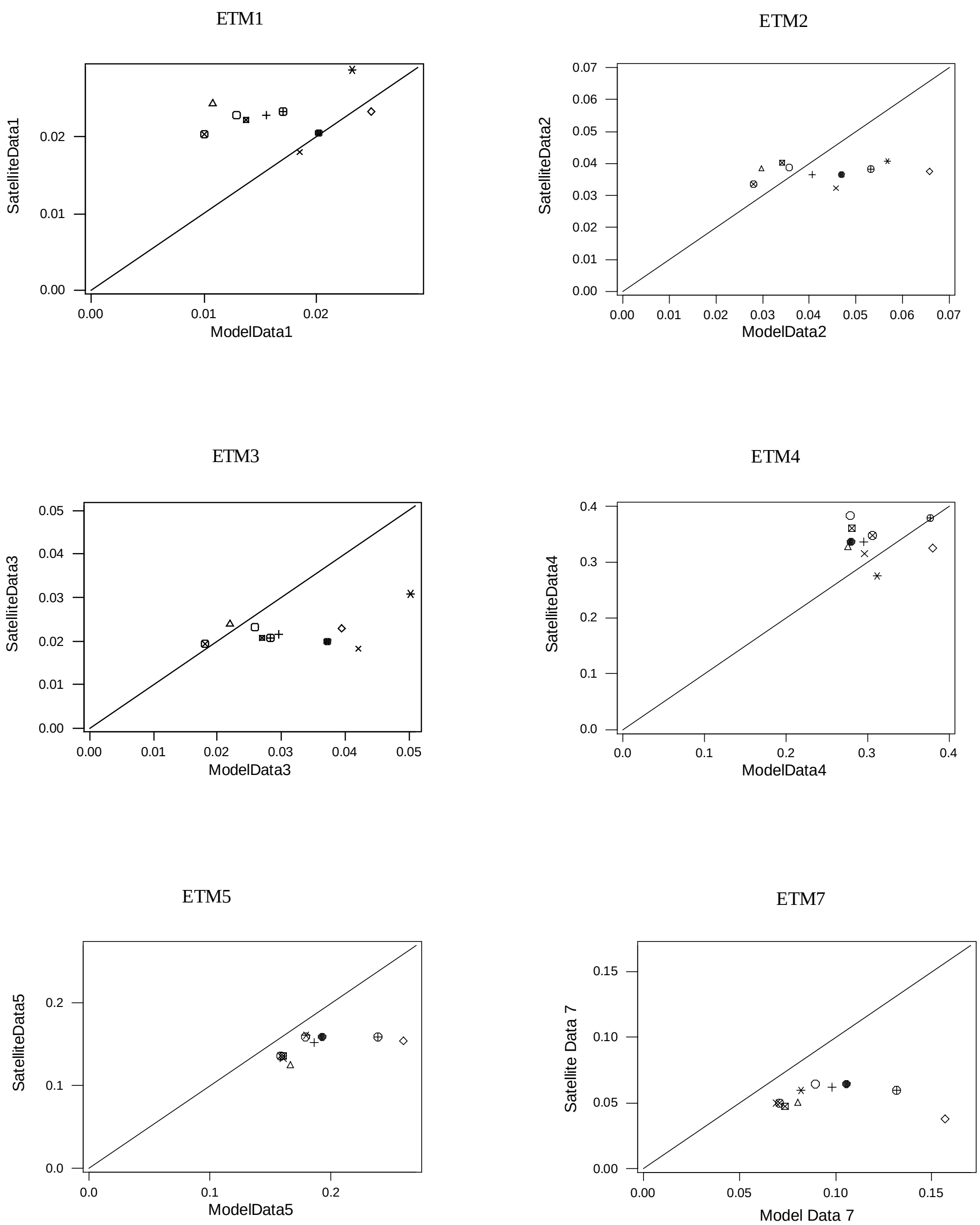

Figure 16-21. Correlation between measured and modelled reflectance (with LAI values recalculated according to Chen), where: • = FT1; ⊕ = Skrylle4; ⊗ = SH5; ⊠ = SH6; × = FT3; + =SH2; ∗ = SH4; O =SH1; ◇ = Torup1; △ = Skrylle8;

8.3.2. Kucharik corrected data

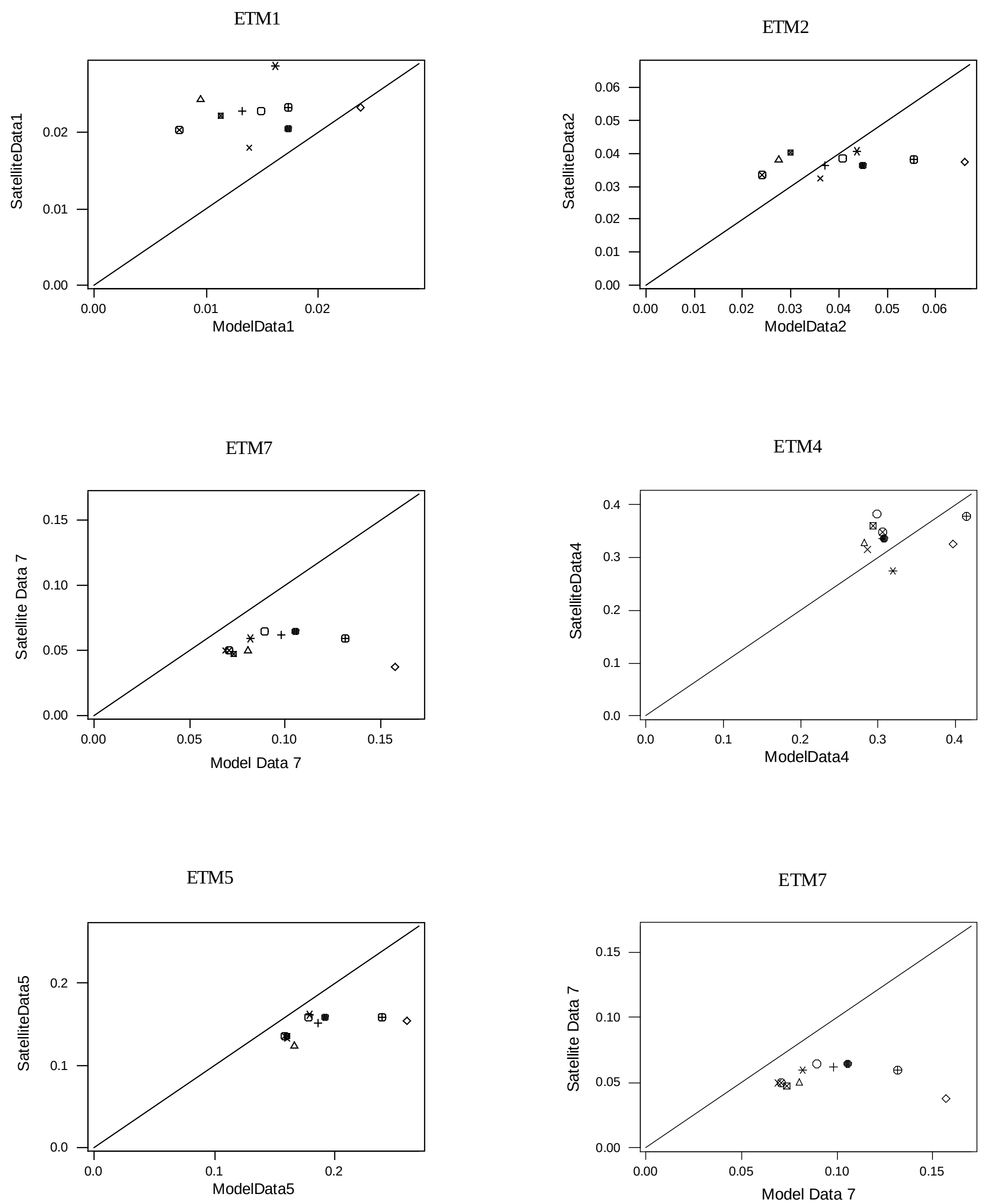

Figure 22-27. Correlation between measured and modelled reflectance (with LAI values recalculated according to Kucharik), where: • = FT1; ⊕ = Skrylle4; ⊗ = SH5; ⊠ = SH6; × = FT3; + =SH2; ∗ = SH4; O =SH1; ◇ = Torup1; △ = Skrylle8;

8.4. Model inversion results

To establish which channels should be used in the inversion a test was made on the FT1 collection. An increased number of channels were used as input to the model. Inversion of ETM 4 only with increasing number of channels to ETM 4+3+2 yielded very low values of LAI. However, using all bands in the visible region and NIR estimated LAI to 1.49. This is to be compared to a measured value of 1.68 (using Chen's adjustment method). The use of ETM 5 and ETM 7 resulted in a better estimate of LAI.

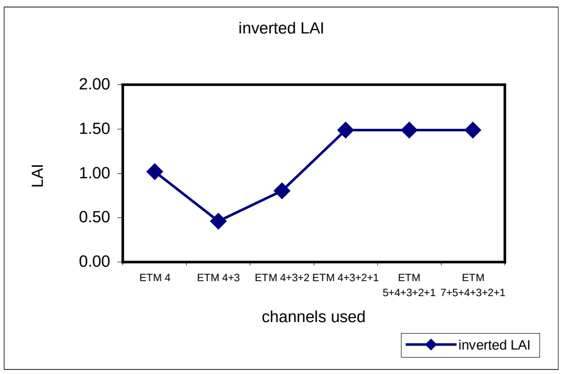

Figure 28. The variation of the inverted LAI with varying number of channels.

Inverting all collections with LAI and BAI as free parameters yields low correlations. In the collections with several classes only the parameters of the first class is inverted. Therefore the assignment of parameter values to the subclasses has very large impact on the inversion results. Furthermore, the actual value of LAI and BAI in a subclass is only estimated with the DBH total-DBH ratio. The inversion result of the multi-class collections is generally low while the one-class collections are better. Plotting only those collections with one class (FT1, T1, SH4) gives an almost linear relationship, see figure 29.

Table 8. Correlations and differences between inverted LAI and measured LAI.

Collection	Inverted LAI	LAI Chen	diff. Chen	LAI Kucharik	diff. Kucharik
FT1	1.49	1.77	0.28	2.64	1.15
SH1	1.3	3.44	2.14	4.3	3.00
SH2	1.66	2.38	0.72	3.08	1.42
FT3	2.43	2.71	0.28	3.34	0.91
SH4	0.53	0.85	0.32	1.28	0.75
SH5	1.01	2.89	1.88	3.58	2.57
SH6	1.23	1.87	0.64	2.54	1.31
S4	2.19	4.07	1.88	4.87	2.68
T1	2.72	2.47	(-) 0.25	3.47	0.75
S8	1.55	3.36	1.81	4.16	2.61
		r=0.458	**mean=0.97**	**r=0.509**	**mean=1.71**

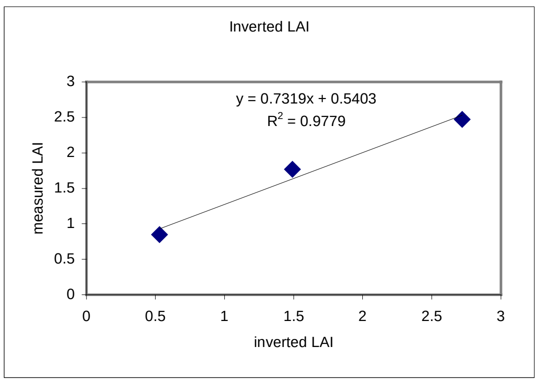

Figure 29. Inversion results for the stands with one size class.

8.5. Relations between satellite measured reflectance and LAI

The relationship between reflectance indices and measured LAI yielded moderate correlation.

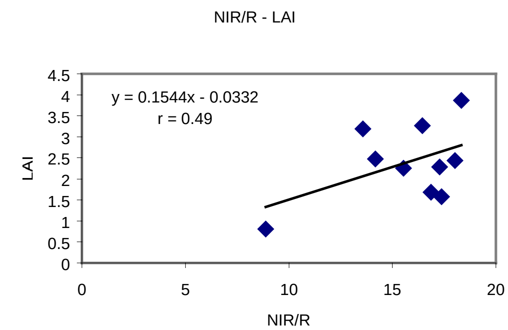

Figure 30. Relations between LAI and NIR/RED

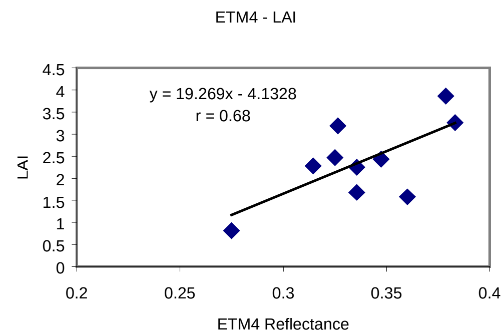

Figure 31. Relations between LAI and ETM 4

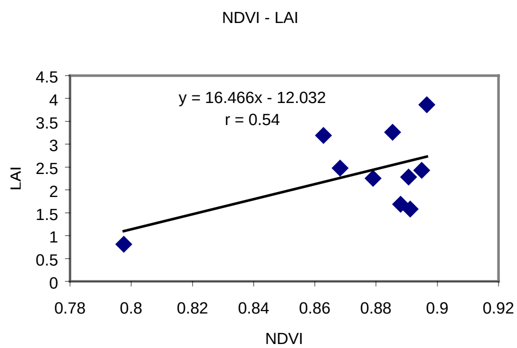

Figure 32. Relations between LAI and NDVI

The plots in figure 30 - 32 shows the relationships between ground measured LAI and satellite-measured reflectance in ETM 4 or reflectance indices. These results should be compared to the results of the model inversion to see if these traditional methods yield better result than reflectance modelling. This method yields similar correlation coefficients as the model inversion.

9. Discussion and conclusions

The need for an atmospheric correction, for these kinds of studies, is emphasized by e.g. Nilson and Peterson (1991). This is the main reason why we have performed an atmospheric correction. Although our results seem to be realistic, we cannot be sure that they are correct. However, we have found no indications that the 6S model is not valid and we have been given a high quality set of input data by the SMHI. Therefore, we have reason to believe that the correction for the atmospheric influence has been successful.

The sensitivity analysis shows that the structural parameters are important in all wavelengths, especially the crown radius, which was shown to be the most important. The chlorophyll content has shown to be of great importance in the visible wavelengths. In addition, the EWT has no importance in the visible region of the spectrum, but is important in the longer wavelengths.

One expected feature shown by the sensitivity analysis is that the understory vegetation increases in importance with decreasing canopy closure. Because understory vegetation data is hard to find, and rather hard to collect, one can assume that reflectance modelling of collections with low canopy closure is more complicated. Kuusk (2000) means that this is also the case with conifer forests.

The low correlations of the reflectance modelling correspond to results presented by Kuusk (2000) where the calculated reflectance deviates from measured reflectance. The main problem for the model is according to Kuusk (2000) in the NIR region (830-1300 nm), which corresponds to our results. However, the modelling done by Kuusk (2000) for conifer forests strongly overestimates the reflectance in NIR while our result, in most cases, underestimate reflectance in NIR for deciduous forest. Kuusk states that this inability of the model to accurately calculate the reflectance in NIR is due to:

- Underestimation of leaf NIR absorption in NIR by the PROSPECT2 model
- The violation of energy conservation law in the model
- Some mechanism of the NIR absorption in the forest model that is not accurately described

The model is able to simulate the reflectance from a forest collection with moderate success. Although we have an accurate set of field data there seems to be to many unknown parameters for the model to perform well. However, the model is a useful tool for sensitivity analysis and to comprehend what parameters are important in forming the satellite signal.

Some conclusions about the two methods for recalculation of the LAI-2000 measurements can be drawn. First, it is obvious when studying table 8 that the LAI values recalculated according to Chen, agrees better with inverted LAI. On average, the difference is 0.97 compared with 1.71 for the LAI values recalculated according to Kucharik. When comparing the satellite reflectance with the modelled reflectance the differences between the two methods are not that large (table 7), with two exceptions: in ETM 3 the Chen method gives an r=0.44, while the Kucharik method only gives an r=0.22. In ETM 4 the Chen method gives an almost zero-correlation. This is however in the model's problematic region (Kuusk, 2000) and the low correlation is probably due to other factors (see sources of errors below). It is hard to say which one of the two methods that calculates the most realistic LAI values. We have found that the Chen recalculation method gives the best result compared to the inverted LAI values. Therefore, we suggest that Chen recalculation method is used in these kinds of studies. However, LAI measurements by litter fall traps should be done to evaluate the LAI-2000 and its correction procedures.

The inversion yielded mixed results. If we only invert the collections with one size class, the inversion is successful. This could be due to the non-complex structure of these collections, which results in accurate field data due to easy measurements. The other collections, with several size classes and hence complex collection architecture, makes field measurements complicated and in some cases full of errors.

9.1. Sources of errors

There are several other reasons for the low correlation between the modelled reflectance and the atmospherically corrected satellite data. The most important may be:

1. Field measurement procedure. The structural parameters may be correct due to homogeneity of trees in respect to shape. However, the density may be wrong due to the small sample area. Too few trees are included in the circle to get a representative value of the collection density. In addition, small errors in field measurements of each parameter may accumulate to large errors in modelling results (Kuusk and Nilson, 2000).
2. The Lopex data set may not valid for Swedish conditions. The data set was developed based on field measurements made in Italy. The actual values of leaf biophysical parameters in our collections may be very different.
3. No actual value of leaf structural parameter is used. Values are taken from literature for aspen trees. No values for our species are found in the literature. In most cases we have used N = 2.5. A 20% increase in this value (i.e. N = 3.0) affects the reflectance much, see sensitivity analysis. Jacquemoud *et al.* (1996) reports values of N from 1.2 to 5.9 for the LOPEX data set (no species specified). Thus, a value of 3.0 may be just as correct as 2.5. Bicheron and Leroy (1999) report a value of 2.64 for aspen and this is the only value found for deciduous forests. However, an approximate value of the parameter may be derived by inverting the PROSPECT model with reflectance values for each species found in the LOPEX data set.
4. Understory vegetation has large impact on collections with low canopy closure. Therefore, better data on understory vegetation is required when modelling low canopy closure collections. The data reported by Nilson *et al.* (2000) are not valid in cases with low hazel bushes, black- and raspberry, which is often the case in southern Sweden. The understory needs more attention according to Kuusk (2000), especially in conifer forests but also in sparse deciduous forests. The understory is a complex plant community composed of different tree, shrub and herb species. In addition, there is often a considerable contribution of litter and sometimes bare soil.
5. The Li-Cor LAI-2000 adjustment procedure. Even though the equations may be valid for our collections, the assumption of random or near random distribution of foliage in the canopies can be false. Gower *et al.* (1999) states that random distribution of foliage in a canopy may be valid for many deciduous forests, pastures, grasslands and

agricultural crops, but it is often invalid for open-canopy forests, boreal coniferous and aspen forests. Assuming random distribution of foliage can produce errors in excess of 100 %.

10. References

Ahrens C. D. (1994). ”Meteorology Today, an Introduction to Weather, Climate and the Environment”, West Publishing Company.

Andersson, K. G. (1985). “Lineär algebra”, Studentlitteratur.

Asrar, G., (1989). ”Introduction”, in Theory and Applications of Optical Remote Sensing (Asrar, G., Ed), John Wiley & Sons.

Badhwar, G. D., McDonald, R. B. and Mehta, N. C. (1986). “Satellite-derived leaf-area-index and vegetation maps as input to global carbon cycle models – a hierarchical approach”, *Int. J. Remote Sensing, vol. 7, no. 2, 265-281*.

Bicheron. P. and Leroy. M. (1999). “A Method of Biophysical Parameter Retrieval at Global Scale by Inversion of a Vegetation Reflectance Model”, *Remote Sens. Environ. 67:251-266.*

California Geodetic Control Committee glossary of GPS terminology. http://www.rbf.com/cgcc/glossary.htm

Campbell, J. B. (1996). “Introduction to Remote Sensing”, Taylor & Francis Ltd.

Chen, J. M., Rich, P. M., Gower, S. T., Norman, J. M. and Plummer, S., (1997), “Leaf area index of boreal forests: Theory, techniques, and measurements”, *Journal of geophysical research 102:29,429-29,443.*

Considine, D. M., ed. (1989). “Van Nostrand’s Scientific Encyclopedia”, Van Nostrand Reinhold.

Clevers, J. P. G. (1992). “Modelling and synergetic use of optical and microwave remote sensing”, *Netherlands Remote Sensing Board*.

Deering, D. W. (1989). “Field measurements of bi-directional reflectance”, in Theory and Applications of Optical Remote Sensing (Asrar, G., Ed), John Wiley & Sons.

Gao, B. C. and Goetz, F. H. (1995). “Retrieval of equivalent water thickness and Information related to biochemical components of vegetation canopies from AVIRIS data”, *Remote Sens. Environ.* 52:155-162.

Goel, N. S. and Thompson R. L. (1984). “Inversion of Vegetation Canopy Reflectance Models for Estimating Agronomic Variables. III. Estimation Using Only Canopy Reflectance Data as Illustrated by the Suits Model”, *Remote Sens. Environ. 15:223-236.*

Goudie, A., ed. (1988). “The Encyclopedic Dictionary of Physical Geography”, Basil Blackwell Ltd.

Gower, S., Kucharik, C. and Norman, J. (1999). “Direct and Indirect Estimation of Leaf Area Index, f_{APAR}, and Net Primary Production of Terrestrial Ecosystems”. *Remote Sens. of Environ. 70:29-51.*

Hosgood, B., Jacquemoud, S., Andreoli, G., Verdebout, J., Pedrini, G. and Schmuck, G. (1995). “Leaf Optical Properties EXperiment 93 (LOPEX93)”. Joint Reserch Centre / Institute for Remote Sensing Applications, Ispra, Italy.

Jacquemoud, S. and Baret, F. (1990). “PROSPECT: a model of optical properties spectra”. *Remote Sens. Environ. 34:75-91.*

Jacquemoud, S., Ustin, L., Verdebout, J., Schmuck, G., Andreoli, G. and Hosgood, B.

(1996). “Estimating Leaf Biochemistry Using the PROSPECT Leaf Optical Model”. *Remote Sens. Environ. 56:194-202.*

Kaufman, Y. J. (1989). ”The Atmospheric Effect on Remote Sensing and its Correction” in Theory and Applications of Optical Remote Sensing (Asrar, G., Ed), John Wiley & Sons.

Kucharik, C. J., Norman, J. M., Gower, S. T. (1998). ”Measurements of branch area and adjusting leaf area index indirect measurements”, *Agricultural and Forest Meteorology 91:69-88.*

Kuusk, A. (1991). “Determination of Vegetation Canopy Parameters from optical Measurements”, *Remote Sens. Environ. 37:207-218.*

Kuusk, A. (1994). “A Multispectral Canopy Reflectance Model”, *Remote Sens. Environ. 50:75-82.*

Kuusk, A. and Nilson, T. (2000). “A Directional Multispectral Forest Reflectance Model”, *Remote Sens. Environ. 72(2): 244-252.*

Körner, S. and Wahlgren, L. (1993). “Praktisk Statistik”, Studentlitteratur.

Landsat 7 Science Data Users Handbook. http://ltpwww.gsfc.nasa.gov/IAS/handbook/handbook_toc.html

Myneni, R.B., Assrar, G. and Kanemasu, E. T. (1989). ”The Theory of Photon Transport in Leaf Canopies” in Theory and Applications of Optical Remote Sensing (Asrar, G., Ed), John Wiley & Sons.

Nilson, T., Lang, M., Kuusk. A., Anniste, J. and Lukk, T. (2000). "Forest reflectance model as an interface between satellite images and forestry databases". Tartu Observatory, 61602 Toravere, Tartumaa, Estonia. Rogow 99 Conference. http://rogow99.sggw.waw.pl/09_session_5/03

Nilson, T. and Peterson, U. (1991). "A Forest Canopy Reflectance Model and a Test Case". *Remote Sens. Environ. 37:131-142*.

Sellers, P. J. (1989), "Vegetation-Canopy Spectral Reflectance and Biophysical Processes" in Theory and Applications of Optical Remote Sensing (Asrar, G., Ed), John Wiley & Sons.

Storvik, G. (1986). "Estimering av parametre i en lineært strukturert kovariansmatrise anvendt i fjeranalyse", Hovedoppgave i statistikk ved Universitetet i Oslo, Norsk Regnesentral, Rapport nr. 782.

Stull, R. B. (1995). "Meteorology Today For Scientists and Engineers, A Technical Companion Book", West Publishing Company.

UCL department of Geography Staff Homepages. http://www.geog.ucl.ac.uk/~plewis/

Vermote, E. F., Tanré, D., Deuzé, J. L., Herman, M. and Morcette, J. (1997a). "6S User Guide Version 2, Second Simulation of the Satellite Signal in the Solar Spectrum (6S)", University of Maryland/ Laboratoire d'Optique Atmospherique.

Vermote, E. F., Tanré, D., Deuzé, J. L., Herman, M. and Morcette, J. (1997b). "Second Simulation of the Satellite Signal in the Solar Spectrum (6S)", *IEEE Transactions on Geosience and Remote Sensing*, 35: 675-686.

Welles J. M. and Norman J. M. (1991). "Instrument for Indirect Measurement of Canopy Architecture", *Agronomy Journal 83:818-825*.

Wolley, J. T. (1973). "Change of leaf dimensions and air volume with change in water content", *Plant Physiology* 41: 815-816.

10.1. Software used in the study

PCI (GCPWorks/Xpace/Imageworks), Version 6.3. PCI

ArcView GIS Version 3.1. ESRI Inc.

Minitab Release 12.1. Minitab Inc.

Office 2000. Microsoft Corporation

Appendixes

Appendix 1: Input.txt

Input.txt

```
7
7 11 10.0 12.95 55.6
8                              (USER'S  MODEL)
1.912 0.311                    (UH2O(G/CM2) ,UO3(CM-ATM))
2                              (AEROSOLS MODEL)
0                              (NEXT VALUE IS THE AERO. OPT. THICK. @550nm)
0.057429156                    (AERO. OPT. THICK. @550nm)
-0.1                           (TARGET ALTITUDE IN KM)
-1000                          (SATELLITE CASE)
0                              (landsat tm)
2.08 2.335                     (bandgränser)
0                              (HOMOGENEOUS CASE)
0                              (DIRECTIONNAL EFFECTS)
1                              (lakew, Target surface)
-0.067710332
```

Appendix 2: Output file 37b7.txt

Output file 37b7s.txt

```
******************************* 6s version 4.1 ****************************** *
*                                                                              *
*                       geometrical conditions identity                        *
*                       -------------------------------                        *
*                       t.m.     observation                                   *
*                month:  7 day :  11 universal time: 10.00 (hh.dd)             *
*               latitude:   55.60 deg        longitude:   12.95 deg            *
*   solar zenith angle:   36.19 deg  solar azimuthal angle:      150.31 deg    *
*   view zenith angle:     0.00 deg  view azimuthal angle:         0.00 deg    *
*   scattering angle:    143.81 deg  azimuthal angle difference: 150.31 deg    *
*                                                                              *
*                       atmospheric model description                          *
*                       -----------------------------                          *
*           atmospheric model identity :                                       *
*             user defined water content : uh2o= 1.912 g/cm2                   *
*             user defined ozone content : uo3 = 0.311 cm-atm                  *
*           aerosols type identity :                                           *
*                      Maritime aerosols model                                 *
*           optical condition identity :                                       *
*                visibility :127.45 km  opt. thick. 550nm : 0.0574             *
*                                                                              *
*                       spectral condition                                     *
*                       ------------------                                     *
*           constant                                                           *
*               value of filter function :                                     *
*                wl inf= 2.080 mic   wl sup= 2.335 mic                         *
*                                                                              *
*                       target type                                            *
*                       -----------                                            *
*           homogeneous ground                                                 *
*             spectral vegetation ground reflectance 0.216                     *
*                                                                              *
*                       target elevation description                           *
*                       ----------------------------                           *
*           ground pressure  [mb] 1000.93                                      *
*           ground altitude  [km] 0.100                                        *
*                gaseous content at target level:                              *
*                uh2o= 1.912 g/cm2        uo3= 0.311 cm-atm                    *
*                                                                              *
*                        atmospheric correction activated                      *
*                        --------------------------------                      *
*           input apparent reflectance :  0.063                                *
*                                                                              *
```

```
*******************************************************************************



*******************************************************************************
*                                                                             *
*                         integrated values of  :                             *
*                         --------------------                                *
*       apparent reflectance  0.1957    appar. rad.(w/m2/sr/mic)      3.987   *
*                   total gaseous transmittance  0.899                        *
*                                                                             *
*******************************************************************************
*                                                                             *
*                         coupling aerosol -wv  :                             *
*                         --------------------                                *
*           wv above aerosol :   0.196     wv mixed with aerosol :   0.196    *
*                       wv under aerosol :   0.196                            *
*                                                                             *
*                         int. normalized  values  of  :                      *
*                         ---------------------------                         *
*                      % of irradiance at ground level                        *
*     % of direct  irr.    % of diffuse irr.    % of enviro. irr              *
*               0.953               0.044               0.003                 *
*                       reflectance at satellite level                        *
*     atm. intrin. ref.   background  ref.  pixel  reflectance                *
*               0.002               0.007               0.187                 *
*                                                                             *
*                         int. absolute values of                             *
*                         -----------------------                             *
*                      irr. at ground level (w/m2/mic)                        *
*     direct solar irr.    atm. diffuse irr.    environment  irr              *
*              57.007               2.639               0.150                 *
*                      rad at satel. level (w/m2/sr/mic)                      *
*     atm. intrin. rad.    background  rad.    pixel  radiance                *
*               0.032               0.144               3.811                 *
*                                                                             *
*                                                                             *
*          int. funct filter (in mic)             int. sol. spect (in w/m2)  *
*             0.2549998                                20.219                 *
*                                                                             *
*******************************************************************************



*******************************************************************************
*                                                                             *
```

```
*                          integrated values of  :                         *
*                          --------------------                            *
*                                                                          *
*                             downward        upward          total        *
*      global gas. trans. :    0.93639        0.94674        0.89887       *
*      water   "     "    :    0.97084        0.97548        0.95424       *
*      ozone   "     "    :    1.00000        1.00000        1.00000       *
*      co2     "     "    :    0.99654        0.99715        0.99417       *
*      oxyg    "     "    :    1.00000        1.00000        1.00000       *
*      no2     "     "    :    0.99827        0.99860        0.99694       *
*      ch4     "     "    :    0.96998        0.97500        0.95156       *
*      co      "     "    :    1.00000        1.00000        1.00000       *
*                                                                          *
*                                                                          *
*      rayl.  sca. trans. :    0.99974        0.99979        0.99953       *
*      aeros. sca.   "    :    0.99584        0.99721        0.99306       *
*      total  sca.   "    :    0.99538        0.99684        0.99224       *
*                                                                          *
*                                                                          *
*                                                                          *
*                             rayleigh       aerosols         total        *
*                                                                          *
*      spherical albedo   :    0.00037        0.01151        0.01158       *
*      optical depth total:    0.00037        0.03989        0.04026       *
*      optical depth plane:    0.00037        0.03989        0.04026       *
*      reflectance        :    0.00017        0.00166        0.00169       *
*      phase function     :    1.22869        0.13495        0.14495       *
*      sing. scat. albedo :    1.00000        0.98488        0.98502       *
*                                                                          *
*                                                                          *
****************************************************************************
****************************************************************************



****************************************************************************
*                        atmospheric correction result                     *
*                        -----------------------------                     *
*       input apparent reflectance            :    0.063                   *
*       measured radiance [w/m2/sr/mic]       :    1.291                   *
*       atmospherically corrected reflectance :    0.069                   *
*       coefficients xa xb xc                 :  0.05504  0.00190  0.01158    *
*       y=xa*(measured radiance)-xb;  acr=y/(1.+xc*y)                      *
****************************************************************************
```

Appendix 3: Standard input file for FT1

```
'BokFulltofta'        : Lai 2
t f                   : lfrt = T - frt, F - ifrt; lprint = T - truki ko~ik
140                   : collection age
1      100            : # size classes, z-levels
filenames of other tree classes:

x0     xmin    xmax                        i
t_elli                : crown form
'bok'                 : species
0.0112 0.116   0.116  : collection density, m-2     2
29.1   14.5    14.5   : tree height, m         3
18     4.1     4.1    : crown l,m ell V con    7
0.                    :      cylinder
5.05   1.      2.4    : crown radius, m        4
57.8   10.     25.    : trunk diameter, cm     6
2.1    4.02    4.02   : leaf area index        1
0.49   0.01    1.     : branch area index      8
1.0    1.25    1.25   : tree distr. param      5
1.00   0.5     0.8    : shoot shading coef     9
41     5.      60.    : chlorophyll content    11
0.0006 0.001   0.01   : protein content        13
0.0014 0.0001  0.01   : lignin & cellulose     14
0.0080 0.01    0.1    : water thickness        15
3.0    1.      2.5    : leaf str. param.       12
1.3                   : refr. ind. ratio'qiltr1.dat'
'qiltr1.dat'          : file of branch reflectance
'qiltr1.dat'          : file of trunk reflectance
0.6    0.01    6.0    : ulgrou                 10
0.2    0.02    0.4    : slgrou                 16
50.0   10.     100.   : cABgrou                17
0.1437 0.05    0.95   : s1_soil                18
0.06   14      9      : shl, nxy, nz
2      0.25    0.25   0.25   0.25   : iaer, c(n) - aerosol data (6S)
127.45 0.0574         : v, tau_aer(550) - visibility (6S)
0.     45.     0.8    0.9    : eln, thm, lmbd_z, n_ratio
0.008  .0015   .008   1.7    : cW, cP, cC, N - ground vegetation
45.    -0.05   0.     0.     : th*, rsl2, rsl3, rsl4
1      100            : # of Sun angles, spectral channels
36.                   : Sun zeniths
450.   20.            : spectrum start and increment
0.     0.             : view nadir and azimuth angles      *** !!! The next lines are not
required for the frtsp  !!!  ***
'powell'              : name of the optimization subroutine
5000   1       500    500    : nfmax, itmax, itbr, nbrak
```

```
1.00E-09       1.00E-07       1.00E-13       1.00E-08       : zeps, tolbr, tiny, ftolp
1.      0.5     2.      0.2     : alpha, beta, gamma, dx
1       10.     f       : n, at, lig - which initial guess
1       2       3               : ll
672.    -1.     -1.     0.0140          th_Sun=30.
802.    -1.     -1.     0.1502          th_Sun=30.
672.    -1.     -1.     0.0129          th_Sun=40.
802.    -1.     -1.     0.1461          th_Sun=40.
672.    -1.     -1.     0.0126          th_Sun=45.
802.    -1.     -1.     0.1451          th_Sun=45.
****|****|****|****|****|****|****|****|****|****|****|****|****|****|****|****|
        total   diffuse nadir
lambda  transmittance   reflectance
```

The reports are available at the Geo-Library, Department of Physical Geography,

University of Lund, Sölvegatan 13, S-223 62 Lund, Sweden.

1. Pilesjö, P. (1985): Metoder för morfometrisk analys av kustområden.
2. Ahlström, K. & Bergman, A. (1986): Kartering av erosionskänsliga områden i Ringsjöbygden.
3. Huseid, A. (1986): Stormfällning och dess orsakssamband, Söderåsen, Skåne.
4. Sandstedt, P. & Wällstedt, B. (1986): Krankesjön under ytan - en naturgeografisk beskrivning.
5. Johansson, K. (1986): En lokalklimatisk temperaturstudie på Kungsmarken, öster om Lund.
6. Estgren, C. (1987): Isälvsstråket Djurfälla-Flädermo, norr om Motala.
7. Lindgren, E. & Runnström, M. (1987): En objektiv metod för att bestämma läplanteringars läverkan.
8. Hansson, R. (1987): Studie av frekvensstyrd filtringsmetod för att segmentera satellitbilder, med försök på Landsat TM-data över ett skogsområde i S. Norrland.
9. Matthiesen, N. & Snäll, M. (1988): Temperatur och himmelsexponering i gator: Resultat av mätningar i Malmö.

10A. Nilsson, S. (1988): Veberöd. En beskrivning av samhällets och bygdens utbyggnad och utveckling från början av 1800-talet till vår tid.
10B. Nilson, G., 1988: Isförhållande i södra Öresund.
11. Tunving, E. (1989): Översvämning i Murciaprovinsen, sydöstra Spanien, november 1987.
12. Glave, S. (1989): Termiska studier i Malmö med värmebilder och konventionell mätutrustning.
13. Mjölbo, Y. (1989): Landskapsförändringen - hur skall den övervakas?
14. Finnander, M-L. (1989): Vädrets betydelse för snöavsmältningen i Tarfaladalen.
15. Ardö, J. (1989): Samband mellan Landsat TM-data och skogliga beståndsdata på avdelningsnivå.
16. Mikaelsson, E. (1989): Byskeälvens dalgång inom Västerbottens län. Geomorfologisk karta, beskrivning och naturvärdesbedömning.
17. Nhilen, C. (1990): Bilavgaser i gatumiljö och deras beroende av vädret. Litteraturstudier och mätning med DOAS vid motortrafikled i Umeå.
18. Brasjö, C. (1990): Geometrisk korrektion av NOAA AVHRR-data.
19. Erlandsson, R. (1991): Vägbanetemperaturer i Lund.
20. Arheimer, B. (1991): Näringsläckage från åkermark inom Brååns dräneringsområde. Lokalisering och åtgärdsförslag.
21. Andersson, G. (1991): En studie av transversalmoräner i västra Småland.

22A. Skillius, Å., (1991): Water havesting in Bakul, Senegal.
22B. Persson, P. (1991): Satellitdata för övervakning av höstsådda rapsfält i Skåne.
23. Michelson, D. (1991): Land Use Mapping of theThat Luang - Salakham Wetland, Lao PDR, Using Landsat TM-Data.
24. Malmberg, U. (1991): En jämförelse mellan SPOT- och Landsatdata för vegetationsklassning i Småland.
25. Mossberg, M. & Pettersson, G. (1991): A Study of Infiltration Capacity in a Semiarid Environment, Mberengwa District, Zimbabwe.

26. Theander, T. (1992): Avfallsupplag i Malmöhus län. Dränering och miljöpåverkan.
27. Osaengius, S. (1992): Stranderosion vid Löderups strandbad.
28. Olsson, K. (1992): Sea Ice Dynamics in Time and Space. Based on upward looking sonar, satellite images and a time series of digital ice charts.
29. Larsson, K. (1993): Gully Erosion from Road Drainage in the Kenyan Highlands. A Study of Aerial Photo Interpreted Factors.
30. Richardson, C. (1993): Nischbildningsprocesser - en fältstudie vid Passglaciären, Kebnekaise.
31. Martinsson, L. (1994): Detection of Forest Change in Sumava Mountains, Czech Republic Using Remotely Sensed Data.
32. Klintenberg, P. (1995): The Vegetation Distribution in the Kärkevagge Valley.
33. Hese, S. (1995): Forest Damage Assessment in the Black Triangle area using Landsat TM, MSS and Forest Inventory data.
34. Josefsson, T. och Mårtensson, I. (1995). A vegetation map and a Digital Elevation Model over the Kapp Linné area, Svalbard -with analyses of the vertical and horizontal distribution of the vegetation
35. Brogaard, S och Falkenström, H. (1995). Assessing salinization, sand encroachment and expanding urban areas in the Nile Valley using Landsat MSS data.
36. Krantz, M. (1996): GIS som hjälpmedel vid växtskyddsrådgivning.
37. Lindegård, P. (1996). VINTERKLIMAT OCH VÅRBAKSLAG. Lufttemperatur och kådflödessjuka hos gran i södra Sverige.
38. Bremborg, P. (1996). Desertification mapping of Horqin Sandy Land, Inner Mongolia, by means of remote sensing.
39. Hellberg, J. (1996). Förändringsstudie av jordbrukslandskapet på Söderslätt 1938-1985.
40. Achberger, C. (1996): Quality and representability of mobile measurements for local climatological research.
41. Olsson, M. (1996): Extrema lufttryck i Europa och Skandinavien 1881-1995
42. Sundberg, D. (1997): En GIS-tillämpad studie av vattenerosion i sydsvensk jordbruksmark.
43. Liljeberg, M. (1997): Klassning och statistisk separabilitetsanalys av marktäckningsklasser i Halland, analys av multivariata data Landsat TM och ERS-1 SAR.
44. Roos, E. (1997): Temperature Variations and Landscape Heterogeneity in two Swedish Agricultural Areas. An application of mobile measurements.
45. Arvidsson, P. (1997): Regional fördelning av skogsskador i förhållande till mängd SO_2 under vegetationsperioden i norra Tjeckien.
46. Akselsson, C. (1997): Kritisk belastning av aciditet för skogsmark i norra Tjeckien.
47. Carlsson, G. (1997): Turbulens och supraglacial meandring.
48. Jönsson, C. (1998): Multitemporala vegetationsstudier i nordöstra Kenya med AVHRR NDVI
49. Kolmert, S. (1998): Evaluation of a conceptual semi-distributed hydrological model – A case study of Hörbyån.
50. Persson, A. (1998): Kartering av markanvändning med meteorologisk satellitdata för förbättring av en atmosfärisk spridningsmodell.
51. Andersson, U. och Nilsson, D. (1998): Distributed hydrological modelling in a GIS

perspective – an evaluation of the MIKE SHE model.
52. Andersson, K. och Carlstedt, J. (1998): Different GIS and remote sensing techniques for detection of changes in vegetation cover - A study in the Nam Ngum and Nam Lik catchment areas in the Lao PDR.
53. Andersson, J., (1999): Användning av global satllitdata för uppskattning av spannmålsproduktion i västafrikanska Sahel.
54. Flodmark, A.E., (1999): Urban Geographic Information Systems, The City of Berkeley Pilot GIS
55A. Lyborg, Jessic & Thurfell, Lilian (1999): Forest damage, water flow and digital elevation models: a case study of the Krkonose National Park, Czech Republic.
55B. Tagesson, I., och Wramneby, A., (1999): Kväveläckage inom Tolångaåns dräneringsområde – modellering och åtgärdssimulering.
56. Almkvist, E., (1999): Högfrekventa tryckvariationer under de senaste århundradena.
57. Alstorp, P., och Johansson, T., (1999): Översiktlig buller- och luftföroreningsinventering i Burlövs Kommun år 1994 med hjälp av geografiska i informationssystem – möjligheter och begränsningar.
58. Mattsson, F., (1999): Analys av molnklotter med IRST-data inom det termala infraröda våglängdsområdet
59. Hallgren, L., och Johansson, A., (1999): Analysing land cover changes in the Caprivi Strip, Namibia, using Landsat TM and Spot XS imagery.
60. Granhäll, T., (1999): Aerosolers dygnsvariationer och långväga transporter.
61. Kjellander, C., (1999): Variations in the energy budget above growing wheat and barley, Ilstorp 1998 - a gradient-profile approach
62. Moskvitina, M., (1999): GIS as a Tool for Environmental Impact Assessment - A case study of EIA implementation for the road building project in Strömstad, Sweden
63. Eriksson, H., (1999): Undersökning av sambandet mellan strålningstemperatur och NDVI i Sahel.
64. Elmqvist, B., Lundström, J., (2000): The utility of NOAA AVHRR data for vegetation studies in semi-arid regions.
65. Wickberg, J., (2000): GIS och statistik vid dräneringsområdesvis kväveläckagebeskrivning i Halland
66. Johansson, M., (2000): Climate conditions required for re-glaciation of cirques in Rassepautasjtjåkka massif, northern Sweden.
67. Asserup, P., Eklöf, M., (2000): Estimation of the soil moisture distribution in the Tamne River Basin, Upper East Region, Ghana.
68. Thern, J., (2000): Markvattenhalt och temperatur i sandig jordbruksmark vid Ilstorp, centrala Skåne: en mätnings- och modelleringsstudie.
69. Andersson, C., Lagerström, M., (2000): Nitrogen leakage from different land use types - a comparison between the watersheds of Graisupis and Vardas, Lithuania.
70. Svensson, M., (2000): Miljökonsekvensbeskrivning med stöd av Geografiska Informationssystem (GIS) – Bullerstudie kring Malmö-Sturup Flyplats.
71. Hyltén, H.A., Uggla, E., (2000): Rule.Based Land Cover Classification and Erosion Risk Assessment of the Krkonoše National Park, Czech Republic.
72. Cronquist, L., Elg, S., (2000): The usefulness of coarse resolution satellite sensor data for identification of biomes in Kenya.

73. Rasmusson, A., (2000): En studie av landskapsindex för kvantifiering av rumsligalandskapsmönster.
74. Olofsson, P., Stenström, R., (2000): Estimation of Leaf Area Index in Southern Sweden with Optical Modelling and a Landsat 7 ETM+ Scene.